The SP140-RESIST pathway regulates interferon mRNA stability and antiviral immunity

Kristen C. Witt[1,2], Adam Dziulko[3], Joohyun An[1,2], Ophelia Vosshall Lee[1,2], Grace Liu[1,2], Azra Lari[2], Roberto Chavez[1,2], David J. Turner[4], Arthur Cheng[1,2], Dmitri I. Kotov[1,2], Preethy Abraham[1,2], Angus Y. Lee[5], Harmandeep Dhaliwal[5], Laurent Coscoy[1,2], Britt Glaunsinger[2,6,7], Edward B. Chuong[3], Russell E. Vance[1,2,5,6]

[1]Division of Immunology and Molecular Medicine, University of California, Berkeley, CA, USA
[2]Department of Molecular and Cell Biology, University of California, Berkeley, CA, USA
[3]Department of Molecular, Cellular, and Developmental Biology and BioFrontiers Institute, University of Colorado Boulder, Boulder, CO, USA
[4]National Cancer Institute, National Institutes of Health, Frederick, MD, USA
[5]Cancer Research Laboratory, University of California, Berkeley, CA, USA
[6]Howard Hughes Medical Institute, University of California, Berkeley, CA, USA
[7]Department of Plant & Microbial Biology, University of California, Berkeley, CA, USA

Abstract

Type I interferons (IFN-Is) are essential for antiviral immunity but must be tightly regulated. The conserved transcriptional repressor SP140 inhibits interferon beta (*Ifnb1*) expression via an unknown mechanism. We find that SP140 does not repress *Ifnb1* transcription but instead negatively regulates *Ifnb1* mRNA stability by directly repressing the expression of a previously uncharacterized regulator we call RESIST (REgulated Stimulator of Interferon via Stabilization of Transcript, previously annotated as Annexin-2 Receptor). RESIST promotes *Ifnb1* mRNA stability by counteracting *Ifnb1* mRNA destabilization mediated by the Tristetraprolin (TTP) family of RNA-binding proteins and the CCR4-NOT deadenylase complex. SP140 localizes within nuclear bodies, punctate structures that play important roles in silencing DNA virus gene expression in the nucleus. Consistent with this observation, we found that SP140 inhibits replication of the gammaherpesvirus MHV68. The antiviral activity of SP140 was independent of its ability to regulate *Ifnb1*. Our results establish dual antiviral and interferon regulatory functions for SP140 and identify the SP140-RESIST pathway as a novel regulator of *Ifnb1* mRNA stability.

Introduction

Type I interferons (IFN-Is) are cytokines that play central roles in antiviral immunity, autoimmunity, and cancer[1-3]. IFN-Is include *Ifnb1* and numerous *Ifna* and other isoforms, which signal through the IFN alpha receptor (IFNAR) to induce hundreds of Interferon Stimulated Genes (ISGs) that counter infection[3,4]. The pathways leading to *Ifnb1* induction have been enumerated in detail[5,6]. However, despite a longstanding appreciation that *Ifnb1* mRNAs turn over rapidly in cells[7], relatively little is known about the pathways controlling *Ifnb1* mRNA stability. This is surprising given that mRNA turnover is a critical point of regulation for many other cytokines[8,9]. In addition, substantial evidence points to the importance of negative regulation of IFN-I, as excessive IFN-I can drive autoimmunity[10] and susceptibility to bacterial infections[6].

SP140 is an evolutionarily conserved but poorly characterized member of the Speckled Protein (SP) family of epigenetic readers that contain histone-recognition and/or DNA-binding domains, as well as an oligomerization domain structurally homologous to caspase-activation and recruitment domains (CARDs)[11,12]. The SP CARD mediates formation of nuclear bodies (NBs)[13], large complexes that mediate various nuclear functions including transcriptional regulation[11,14]. The functions of SP140 are unclear, although previous work suggests SP140 is a transcriptional repressor essential for macrophage and possibly T-cell function[11,15-22]. In humans, loss-of-function mutations in SP140 are associated with immune disorders such as multiple sclerosis and B cell cancers[23-28]. We previously found a critical role for SP140 in the repression of IFN-I *in vivo*, as *Sp140*$^{-/-}$ mice are highly susceptible to multiple bacterial infections due to elevated IFN-I[29]. However, the mechanism by which SP140 represses IFN-I is entirely unknown.

Results

SP140 is a negative regulator of *Ifnb1* transcript stability

To investigate how SP140 regulates IFN-I, we first characterized *Ifnb1* transcript levels in wild-type C57BL/6J (B6) and *Sp140*$^{-/-}$ bone marrow-derived macrophages (BMMs) stimulated with agonists of distinct IFN-I-inducing pathways, including bacterial lipopolysaccharide (LPS), the dsRNA mimic poly(I:C), and the mouse STING agonist DMXAA (Fig. 1a). We noted that *Ifnb1* transcript levels were similar between B6 and *Sp140*$^{-/-}$ cells at early timepoints (2-4 hours) after stimulation, but remained elevated (~10-fold) in *Sp140*$^{-/-}$ cells at late time points (8 hours) for all IFN-I inducing stimuli (Fig. 1a). A time course of *Ifnb1* transcript levels after DMXAA stimulation confirmed that *Sp140*$^{-/-}$ cells displayed increased *Ifnb1* mRNA at late timepoints after stimulation (8-12 hours) (Fig. 1b).

We hypothesized that the elevated levels of *Ifnb1* mRNA at late time points in *Sp140*$^{-/-}$ BMMs are due to the increased stability of *Ifnb1* transcripts. To assess *Ifnb1* mRNA stability, we used Roadblock RT-qPCR[30], a method in which the nucleotide analog 4-thiouridine (4SU) is added to cells and incorporated into newly transcribed mRNAs. Isolated RNA is then treated with N-ethylmaleimide (NEM), which reacts with 4SU to introduce a sterically bulky group that blocks reverse transcription. By adding 4SU at the peak of *Ifnb1* induction (t=2h after DMXAA stimulation), we could follow the subsequent decay of existing *Ifnb1* mRNA without detecting newly transcribed mRNAs. Using this approach, we found that the decay of *Ifnb1* transcript was markedly delayed in *Sp140*$^{-/-}$ BMMs (Fig. 1c). These results demonstrate an unexpected role for SP140 in the regulation of *Ifnb1* transcript stability.

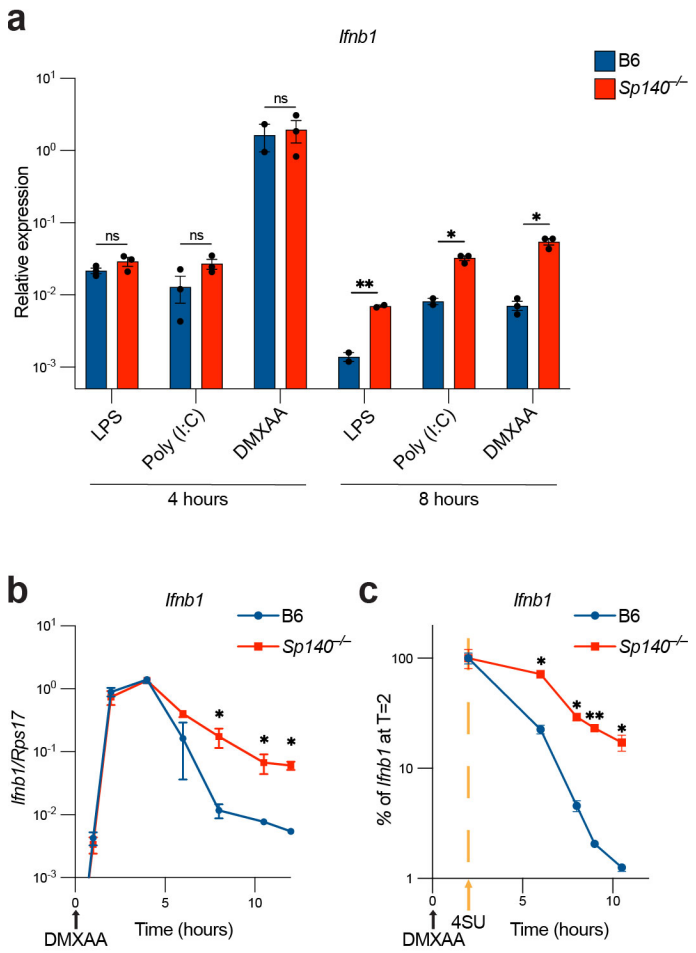

Figure 1. *Ifnb1* mRNA is stabilized in the absence of SP140.

a. *Ifnb1* RT-qPCR in BMMs treated for 4 or 8 hours with 10 ng/mL LPS, or 100 μg/mL poly(I:C) or DMXAA.
b. *Ifnb1* RT-qPCR from BMMs treated with 100 μg/mL DMXAA at indicated timepoints.
c. Roadblock RT-qPCR of BMMs treated with 4SU 2 hours after treatment with 100 μg/mL DMXAA.

SP140 represses expression of *Gm21188* and *Gm36079*

SP140 lacks predicted RNA-binding domains and is believed to act in the nucleus to repress transcription. We therefore hypothesized that SP140 indirectly regulates *Ifnb1* mRNA stability by repressing the transcription of an unknown factor. To identify this factor, we generated RNA-seq data from DMXAA-treated B6 and *Sp140*$^{-/-}$ BMMs, and from DMXAA-treated *Ifnar*$^{-/-}$ and *Sp140*$^{-/-}$*Ifnar*$^{-/-}$ BMMs. The latter dataset eliminates the potentially confounding effects of elevated IFN-I signaling that is otherwise present in *Sp140*$^{-/-}$ BMMs. Surprisingly few genes were differentially expressed between DMXAA-treated *Ifnar*$^{-/-}$ and *Sp140*$^{-/-}$*Ifnar*$^{-/-}$ BMMs (Fig. 2a). Other than *Ifnb1* itself, no known IFN-I regulators were differentially expressed, and gene ontology analysis of

differentially expressed genes (DEGs) did not identify significantly enriched biological processes. Interestingly, only two DEGs correlated with *Ifnb1* upregulation across both RNA-seq datasets (Fig. 2b): *Sp140,* which was downregulated in Sp140-deficient cells, as expected, and *Gm21188*, a poorly annotated gene that was upregulated in SP140-deficient cells. *Gm36079,* a tandem paralog of *Gm21188,* was significantly differentially expressed only in IFNAR-sufficient *Sp140*$^{-/-}$ BMMs treated with DMXAA, suggesting IFNAR signaling is required for robust *Gm36079* induction (Fig. 2b). The open reading frames of *Gm21188* and *Gm36079* differ by a single silent nucleotide substitution and thus encode an identical protein.

To test whether *Gm21188* or *Gm36079* are direct targets of SP140, we performed CUT&RUN[31] with an anti-HA antibody on DMXAA-treated *Sp140*$^{-/-}$ BMMs retrovirally transduced with HA-SP140, or untagged SP140 as a negative control. We confirmed that untagged and HA-tagged SP140 were functional and able to reduce late *Ifnb1* transcript levels induced by DMXAA (Supplemental Fig. 1a). In parallel, to characterize how SP140 regulates chromatin accessibility at target genes, we also generated ATAC-seq data from DMXAA-treated B6 and *Sp140*$^{-/-}$ BMMs. Consistent with previous SP140 ChIP-seq results[17], we found that SP140 binds genetic loci involved in development, such as *Hoxa9* (Supplemental Fig. 1b-d). Similarly, we confirmed SP140 generally represses chromatin accessibility at target genes, consistent with previous studies implicating SP140 in transcriptional repression[16,17,19] (Supplemental Fig. 1c). SP140-binding also correlated with the transcriptionally repressive histone mark H3K27me3 in publicly available ChIP-seq datasets (Supplemental Fig. 1e). However, a gene set previously reported to drive macrophage dysfunction after SP140 knockdown was not significantly upregulated in SP140-deficient BMMs[16,17] (Fig. 2a, Supplemental Fig. 1f), suggesting that these genes do not explain elevated IFN-I induction that occurs in the absence of SP140. Consistent with our hypothesis that SP140 regulates *Ifnb1* mRNA stability and does not directly regulate *Ifnb1* transcription, SP140 did not bind or regulate chromatin accessibility at the *Ifnb1* gene (Supplemental Fig. 2a) or known *Ifnb1* regulatory elements[32-35] (Supplemental Fig. 2b).

Importantly, SP140 robustly bound and repressed chromatin accessibility at the locus containing *Gm21188* and *Gm36079* (Fig. 2b-c). Of the upregulated genes in DMXAA-treated *Sp140*$^{-/-}$*Ifnar*$^{-/-}$ vs. *Ifnar*$^{-/-}$ BMMs, only *Gm21188* was both bound by SP140 and showed increased chromatin accessibility in the absence of SP140 (Fig. 2b-c). SP140 binds a ~10 kb region encompassing *Gm36079* and *Gm21188*, and negatively regulates chromatin accessibility at *Gm36079* and *Gm21188* gene bodies (Fig. 2c). These results demonstrate that *Gm21188* and *Gm36079* are directly repressed by SP140 and are the only direct SP140 target genes upregulated along with *Ifnb1* in *Sp140*$^{-/-}$ cells.

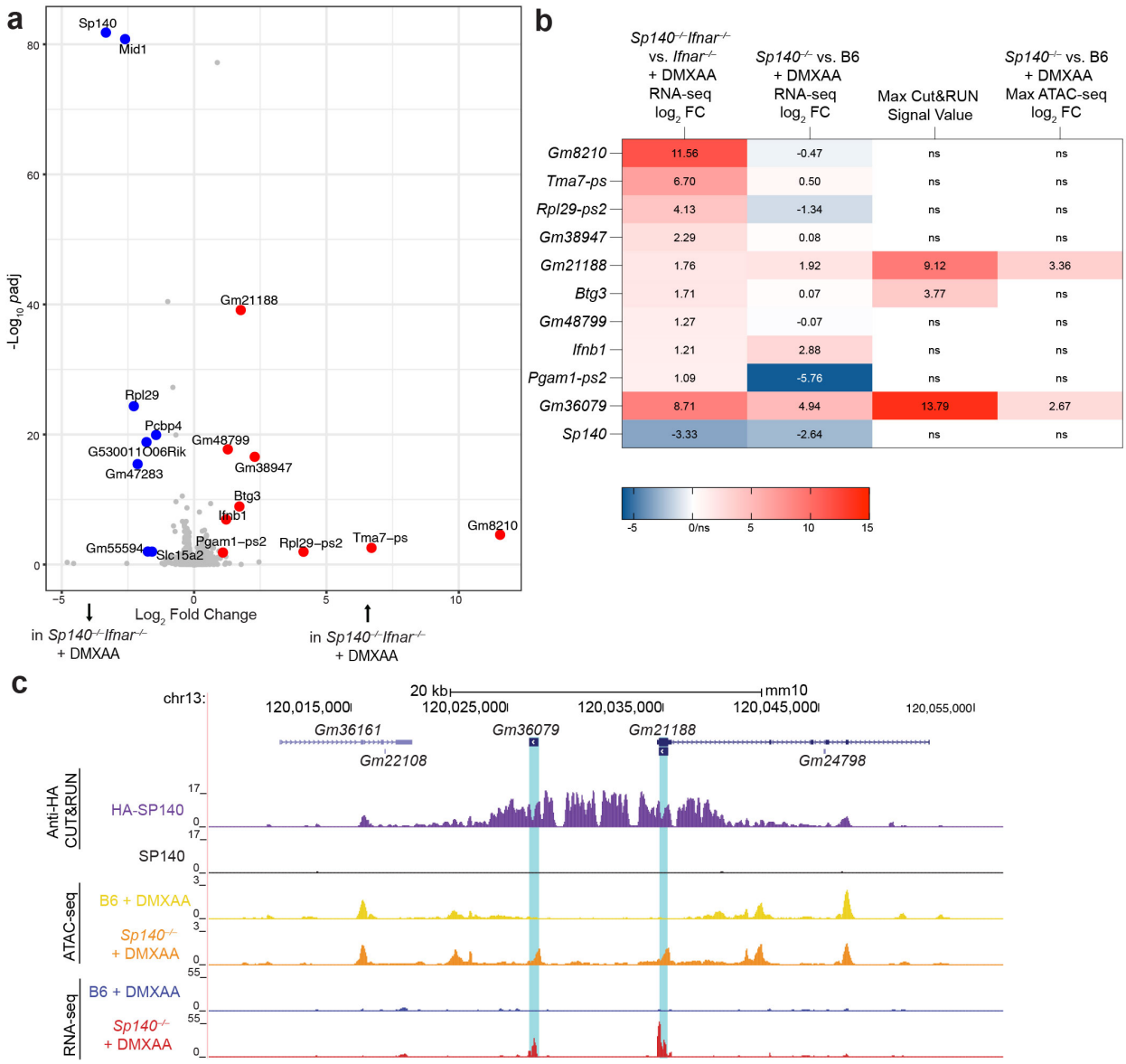

Figure 2. *Gm21188* and *Gm36079* are repressed by SP140 and correlate with increased *Ifnb1* transcript in *Sp140*$^{-/-}$ cells.

a. Volcano plot of differentially expressed genes (DEGs) from RNA-seq of DMXAA-treated *Sp140*$^{-/-}$*Ifnar*$^{-/-}$ vs. *Ifnar*$^{-/-}$ BMMs. Red genes are upregulated in *Sp140*$^{-/-}$ *Ifnar*$^{-/-}$ BMMs with $\log_2$ fold change > 1 and adjusted *p*-value < 0.05. Blue genes are downregulated in *Sp140*$^{-/-}$*Ifnar*$^{-/-}$ BMMs with $\log_2$ fold change > -1 and adjusted *p*-value < 0.05. The adjusted *p*-value for *Sp140* is < 2.225074 e-308 and is graphed as -10*(adjusted *p*-value) of *Mid1* for visualization.

b. Table of maximum HA-SP140 CUT&RUN MACS2 signal value, maximum $\log_2$ fold change in chromatin accessibility from ATAC-seq of DMXAA-treated B6 and *Sp140*$^{-/-}$ BMMs, and $\log_2$ fold change from RNA-seq of DMXAA-treated B6, *Sp140*$^{-/-}$, *Ifnar*$^{-/-}$ and *Sp140*$^{-/-}$*Ifnar*$^{-/-}$ BMMs, for significantly upregulated DEGs

from a, as well as *Sp140* and *Gm36079* (ns = not significant). Cells are colored according to the column value.

c. Alignment of reads at *Gm21188/Gm36079* locus from anti-HA CUT&RUN for DMXAA-treated BMMs transduced with HA-SP140 or SP140, and ATAC-seq/RNA-seq of DMXAA-treated B6 and *Sp140*$^{-/-}$ BMMs. Alignments were visualized in the UCSC genome browser.

_Gm21188_ and _Gm36079_ encode RESIST, which enhances _Ifnb1_ mRNA stability

Gm21188 and *Gm36079* are poorly annotated genes that encode an identical 20.9 kDa protein which is not characterized in mice, but is the ortholog of the human Annexin-2 Receptor (ANXA2R). ANXA2R was first proposed as a receptor for Annexin-2 (ANXA2) based on the observation that ANXA2R overexpression increased the binding of exogenous ANXA2 to the cell surface[36]. However, ANXA2R is not likely to be a cell surface receptor as the DeepTMHMM algorithm[37] fails to predict transmembrane helices. Moreover, recent work using unbiased mass spectrometry of immunoprecipitated human ANXA2R did not identify ANXA2 but instead identified the CCR4-NOT complex as the predominant ANXA2R-binding partner in cells[38]. We also found that a purified recombinant human RESIST protein comprising residues 1-160 (RESIST1-160) did not robustly interact with the ANXA2-S100A complex, whereas a confirmed ANXA2 interaction partner (SMARCA3)[39] was able to bind ANXA2-S100A (Supplemental Fig 3).

CCR4-NOT is the major mRNA deadenylase complex in eukaryotic cells[40,41]. Specific mRNAs targeted for deadenylation are recruited to CCR4-NOT via mRNA-binding proteins (RBPs) that use small peptide motifs to dock to multiple interfaces on CCR4-NOT[40,41]. Recruited mRNAs are subsequently deadenylated, leading to their destabilization and degradation[40,41]. Human ANXA2R was proposed to inhibit CCR4-NOT and appeared to have antiviral effects[38], though the antiviral mechanism was unclear. As a unified hypothesis to explain how SP140 regulates *Ifnb1* mRNA stability and how ANXA2R provides antiviral defense, we propose that Gm21188/Gm36079/ANXA2R stabilize the *Ifnb1* mRNA by binding CCR4-NOT to inhibit *Ifnb1* mRNA recruitment, deadenylation, and decay. Given our data (below) that are consistent with this model, we therefore refer to Gm21188/Gm36079/ANXA2R as RESIST (REgulated Stimulator of Interferon via Stabilization of Transcript), which is encoded in mice by the genes *Resist1* (*Gm21188*) and *Resist2* (*Gm36079*), or in humans by a single *ANXA2R* gene.

We first confirmed that HA-tagged mouse RESIST expressed in primary BMMs co-immunoprecipitated with CNOT1, the major scaffolding protein of CCR4-NOT (Fig. 3a). To test whether RESIST drives elevated *Ifnb1* mRNA levels in *Sp140*$^{-/-}$ BMMs, we disrupted *Resist1/2* genes by Cas9:gRNA electroporation of primary BMMs[42] (Fig. 3b). *Resist1/2* disruption almost entirely eliminated the elevated *Ifnb1* transcript observed in DMXAA-treated *Sp140*$^{-/-}$ BMMs (Fig. 3b). Roadblock RT-qPCR confirmed that the decreased *Ifnb1* mRNA levels seen in *Resist1/2* knockout cells were due to decreased mRNA stability (Fig. 3c). Furthermore, RESIST overexpression in primary BMMs was sufficient to elevate *Ifnb1* transcript levels >10-fold, and eliminated the difference in *Ifnb1* transcript levels between B6 and *Sp140*$^{-/-}$ BMMs (Fig. 3d). RESIST overexpression also promoted *Ifnb1* transcript stabilization in primary BMMs, measured

by Roadblock RT-qPCR (Fig. 3e). Finally, overexpressed human RESIST also drove >10-fold elevated *IFNB1* transcript levels in human BlaER1 monocytes, which do not endogenously express RESIST, upon stimulation with the STING agonist ADU-S100 (Fig. 3f). These results identify mouse and human RESIST as a potent positive regulator of IFN-I.

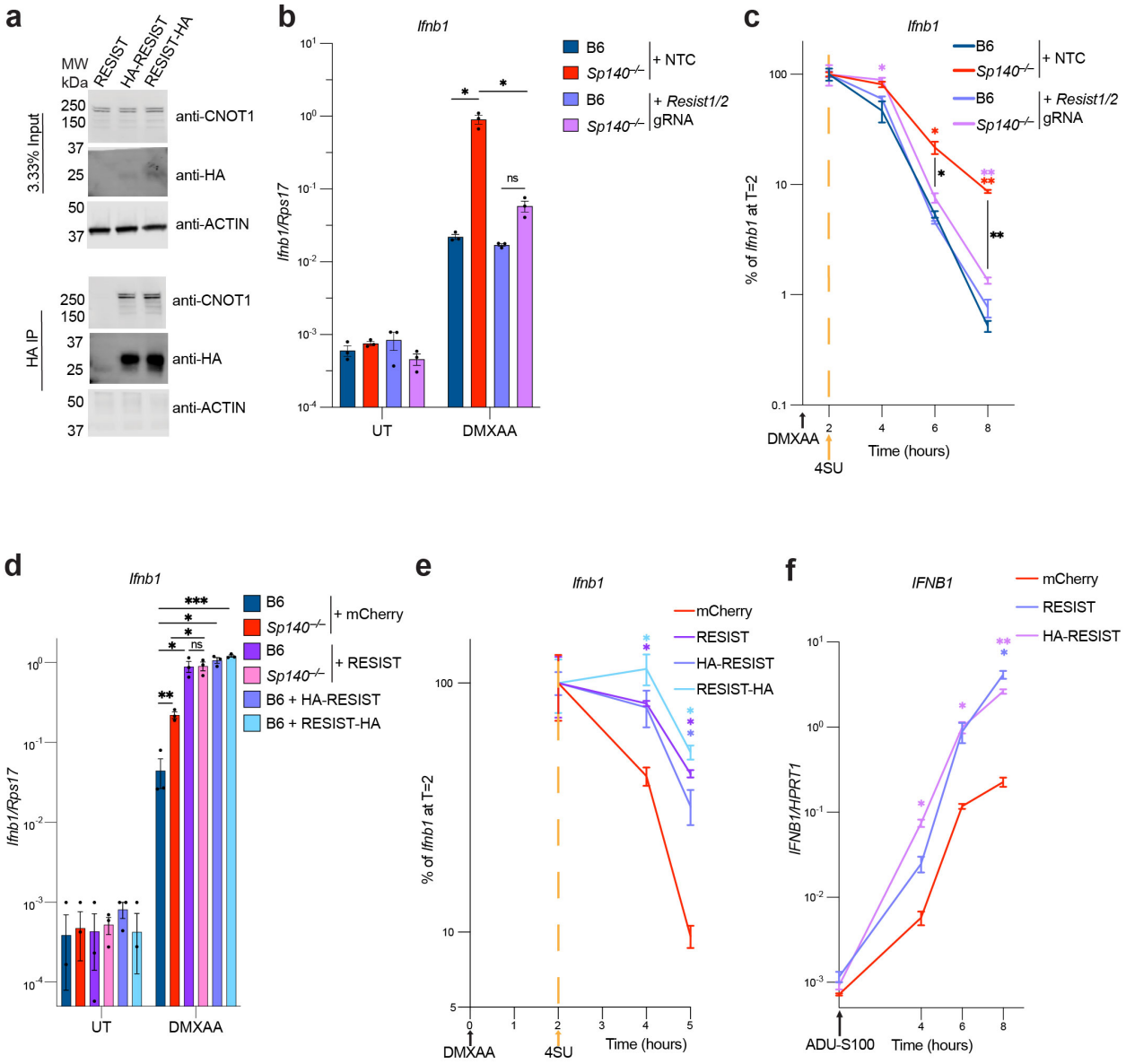

Figure 3. RESIST binds the CCR4-NOT complex and drives *Ifnb1* mRNA stabilization in *Sp140*$^{-/-}$ macrophages.

a. Immunoblot of input lysate or anti-HA immunoprecipitate for BMMs lentivirally transduced with RESIST constructs, stimulated with doxycycline and 100 μg/mL DMXAA for 5-7 hours.
b. *Ifnb1* RT-qPCR from BMMs electroporated with non-targeting control (NTC) or *Resist1/2* gRNA, stimulated for 8 hours with 100 μg/mL DMXAA or untreated

(UT). Knockout efficiency in the experiment shown was 86-87% for *Resist1* and 91% for *Resist2*.

c. Roadblock RT-qPCR of BMMs electroporated with indicated gRNAs and treated with 100 μg/mL DMXAA, followed by 4SU at T2. The estimated knockout efficiency in the experiment shown was 71% for *Resist1* and 51-69% for *Resist2*. Asterisks indicate a significant difference in *Ifnb1* transcript compared to B6 + NTC at each time point and are colored by condition compared to B6 + NTC. Black bars/asterisks indicate a comparison between *Sp140*$^{-/-}$ + NTC and *Sp140*$^{-/-}$ + *Resist1/2* gRNA.
d. *Ifnb1* RT-qPCR from BMMs lentivirally transduced with indicated constructs, treated with doxycycline and 100 μg/mL DMXAA for 7 hours.
e. Roadblock RT-qPCR for *Ifnb1* from B6 BMMs lentivirally transduced with indicated constructs, stimulated with doxycycline and 100 μg/mL DMXAA at T0, followed by 4SU treatment at T2. Asterisks indicate a significant difference in *Ifnb1* compared to mCherry at each time point and are colored by condition compared to mCherry.
f. *IFNB1* RT-qPCR from human BlaER1 monocytes overexpressing human RESIST constructs or mCherry, stimulated with ADU-S100 and doxycycline. Asterisks indicate a significant difference in *IFNB1* transcript compared to mCherry-expressing cells and are colored by RESIST construct compared to mCherry.

RESIST counteracts *Ifnb1* mRNA destabilization mediated by CCR4-NOT and the TTP family of RNA-binding proteins

To elucidate the mechanism by which RESIST stabilizes *Ifnb1* mRNA, we used AlphaFold-Multimer[43] to generate structure predictions of the interaction between mouse RESIST and CCR4-NOT subunits implicated in IFN-I regulation, including 1) CNOT10/11, which recruit RBPs and negatively regulate IFN-I signaling in T-cells[44,45], 2) the CNOT1 M-HEAT, which bind tristetraprolin (TTP), an RBP that has been implicated in negative regulation of *Ifnb1* mRNA stability[46-49], and 3) CNOT9, which acts as a secondary binding site for TTP[50] and was shown to directly bind Roquin1, which, along with Roquin2, negatively regulates transcript stability for pro-inflammatory cytokines[8,51].

Structural predictions suggested that RESIST interacts with multiple sites on the CCR4-NOT complex (Fig. 4a, Supplemental Fig. 4a). Such multivalent interactions are typical of many CCR4-NOT interacting proteins[40]. Intriguingly, the RESIST C-terminal region is predicted to fold into a helix (residues 168-177) and to interact with CNOT1 M-HEAT at the site previously shown to be bound by TTP[46] (Fig. 4a, Supplemental Fig. 4). Moreover, RESIST was predicted to bind the tryptophan binding pockets on CNOT9 known to interact with TTP (Fig. 4a, Supplemental Fig. 5)[50]. Both interactions were characterized by hydrophobic interactions between RESIST and CNOT1/CNOT9, as well as a high number of predicted models and predicted local distance difference test (pLDDT), and low predicted aligned error (PAE) (Supplemental Fig. 4b-e and 5a-d). AlphaFold also predicted, with lower confidence, that the RESIST C-terminal region interacted with a CNOT9 interface bound by *Drosophila* Roquin[51] (Fig. 4a,

Supplemental Fig. 5a-d). In contrast, AlphaFold did not predict a high-confidence interaction between RESIST and CNOT10/11 (Supplemental Fig. 6).

To assess the functionality of CCR4-NOT subunits predicted to interact with RESIST, we genetically disrupted CCR4-NOT subunits (*Cnot1/11/9*) in BMMs with Cas9:gRNA electroporation[42] . We evaluated *Ifnb1* transcript levels by RT-qPCR at the late 8 hr time point after DMXAA stimulation (Fig. 4b). Notably, targeting of the CCR4-NOT scaffold gene *Cnot1* was not well-tolerated, with 5-10-fold fewer cells recovered after electroporation relative to non-targeting controls (NTC), and variable knockout efficiency between experiments. Nevertheless, *Cnot1* deficiency phenocopied RESIST overexpression and led to similarly increased *Ifnb1* upon DMXAA stimulation in both B6 and *Sp140*$^{-/-}$ cells (Fig. 4b), consistent with the hypothesis that RESIST elevates *Ifnb1* transcript levels by inhibition of CCR4-NOT. By contrast, targeting *Cnot11* did not regulate *Ifnb1* in either B6 or *Sp140*$^{-/-}$ BMMs (Fig. 4b, Supplemental Fig. 7a), demonstrating that RESIST-mediated IFN stability does not require CNOT11 and consistent with the absence of evidence for a predicted interaction. Interestingly, deletion of *Cnot9* eliminated elevated *Ifnb1* transcript in DMXAA-stimulated *Sp140*$^{-/-}$ BMMs, but did not affect *Ifnb1* levels in DMXAA-stimulated B6 BMMs (Fig. 4b, Supplemental Fig. 7a). These results indicate CNOT9 is required for RESIST function.

To probe the functional significance of the RESIST C-terminal region, we generated a truncation mutant lacking the region predicted to bind the same site on CNOT1 as TTP (RESIST ΔC). BMMs transduced with the RESISTΔC mutant induced much lower levels of *Ifnb1* transcript than BMMs transduced with WT RESIST (Fig. 4c), suggesting the C-terminal region is essential for RESIST-mediated *Ifnb1* mRNA stabilization. The RESISTΔC mutant immunoprecipitated with the CCR4-NOT complex (Fig. 4d), consistent with a predicted multivalent interaction between RESIST and the CCR4-NOT complex (Fig. 4a).

RESIST is predicted to interact with the known interfaces that TTP and Roquin bind on the CCR4-NOT complex to mediate the decay of their target transcripts. We therefore asked whether TTP and Roquin mediated *Ifnb1* mRNA decay. We disrupted the genes encoding Roquin1/2 (*Rc3h1/2)*, as well as TTP (*Zfp36*) alone and in combination with additional TTP family members (*Zfp36L1, Zfp36L2)*, and evaluated *Ifnb1* transcript levels by RT-qPCR. Genetic disruption of *Rc3h1/2* did not affect *Ifnb1* induced by DMXAA in either B6 or *Sp140*$^{-/-}$ BMMs (Supplemental Fig. 8). By contrast, loss of *Zfp36* in DMXAA-stimulated B6 BMMs increased *Ifnb1* transcript levels (Fig. 4e). However, *Sp140* deficiency further increases *Ifnb1* in the absence of *Zfp36*, implying that RESIST has additional activities beyond TTP inhibition in *Sp140*$^{-/-}$ BMMs (Fig. 4e, Supplemental Fig. 7b). Consistent with this hypothesis, deletion of the genes encoding the additional TTP family members *Zfp36l1/Zfp36l2* resulted in further elevation of *Ifnb1* (Fig. 4e, Supplemental Fig. 7b). These results imply a previously unappreciated role for these TTP family members in negative regulation of *Ifnb1* mRNA stability. Crucially, loss of *Sp140* does not affect *Ifnb1* levels in the absence of the *Zfp36* gene family (Fig. 4e). These results are consistent with a model in which RESIST interferes with the ability of TTP family members to mediate *Ifnb1* transcript destabilization. A potential model consistent with our data is one in which RESIST binds CCR4-NOT and hinders the interaction between the CCR4-NOT complex and TTP family members, leading to the derepression of *Ifnb1* mRNA instability (Supplemental Fig. 9). In contrast, CNOT9,

which is required for elevated *Ifnb1* in *Sp140*$^{-/-}$ cells, appears to promote RESIST function, potentially by facilitating the interaction of RESIST with CCR4-NOT (Fig. 4a, Supplemental Fig. 9). A detailed mechanism for RESIST function will require structural analyses of the RESIST-CCR4-NOT complex.

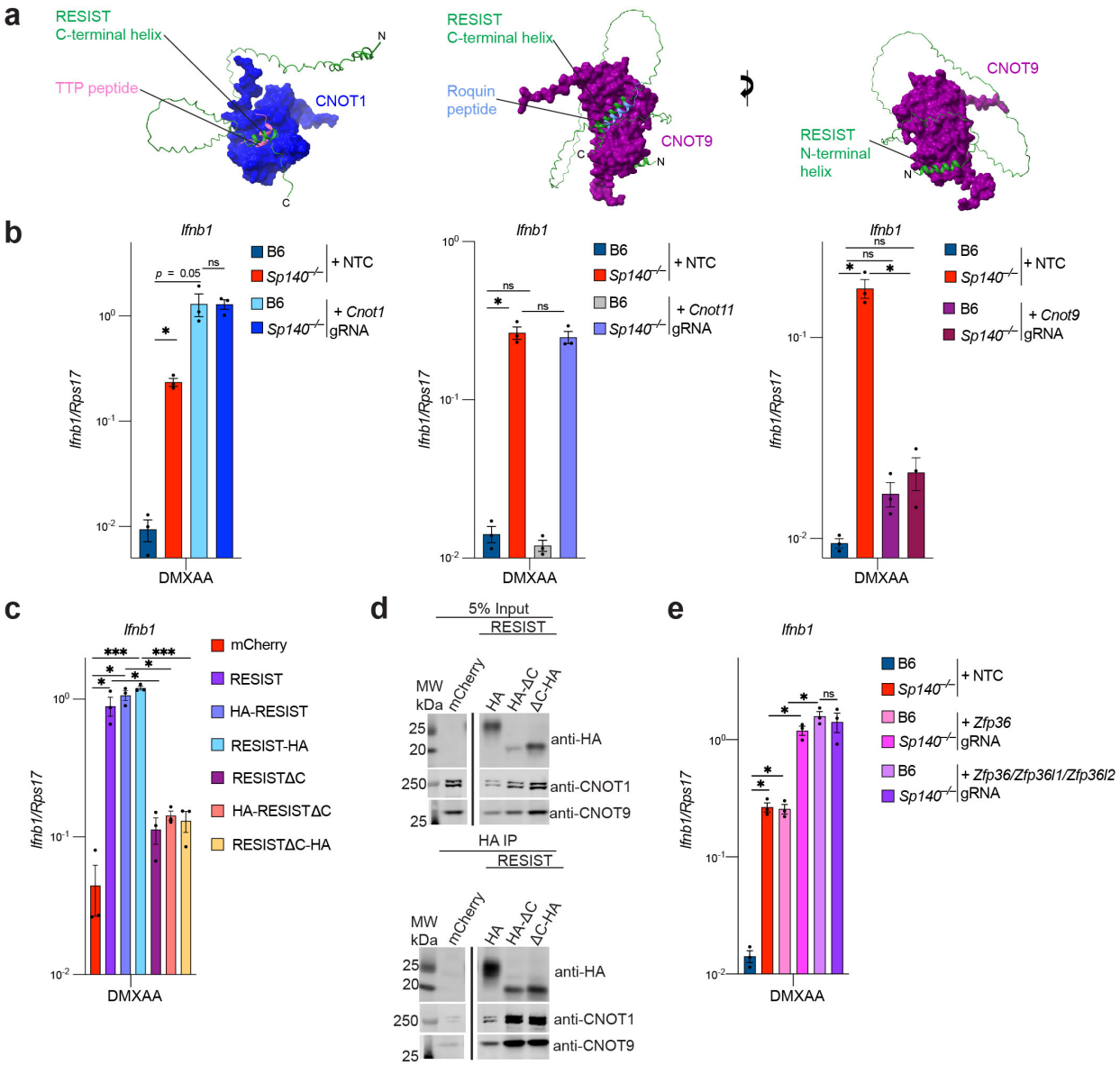

Figure 4. RESIST counteracts repression of IFN-I by TTP family proteins, a function which requires a RESIST C-terminal region and CNOT9

a. AlphaFold predictions of RESIST with CNOT1 M-HEAT and CNOT9. TTP peptide:CNOT1 M-HEAT is PDB code 4J8S[46]. Roquin peptide:CNOT9 is PDB code 5LSW[51]. N and C-terminal ends of RESIST are marked by “N” or “C” respectively.

b. *Ifnb1* RT-qPCR from BMMs electroporated with non-targeting control gRNA (NTC) or gRNAs targeting indicated CCR4-NOT subunits, treated for 8 hours with 100 μg/mL DMXAA.
c. *Ifnb1* RT-qPCR for BMMs lentivirally transduced with indicated constructs, treated with doxycycline and DMXAA for 6 hours. Results include data also shown in Fig. 3d.
d. Immunoblot for anti-HA IP of BMMs transduced with indicated constructs in e. RESIST construct is C-terminally tagged with HA.
e. *Ifnb1* RT-qPCR from BMMs electroporated with indicated gRNAs, treated for 8 hours with 100 μg/mL DMXAA.

Antiviral activity of SP140

Lastly, we considered why SP140 may have evolved to repress the antiviral cytokine IFN-I. Intriguingly, SP140 is part of a family of proteins that includes SP100, a well-described antiviral protein[52]. Mechanistically, SP100 is thought to repress transcription of viral genomes in the nucleus through sequestration in transcriptionally repressive nuclear bodies (NBs) that co-localize with the NB protein PML[52]. SP140 has also been reported to co-localize with PML[53,54], although the composition of SP140 NBs at endogenous expression levels in primary immune cells has not been evaluated with validated SP140-specific antibodies. Similarly, whether SP140 has antiviral activity is unknown. Importantly, because SP100 and other NBs are often antiviral, viruses frequently encode effectors to disrupt NB function[32,52,55,56]. To counter the effector-mediated disruption of NBs, we previously proposed that antiviral NB proteins can evolve the ability to repress IFN-I as a secondary function[32,57]. Thus, viruses that disrupt NBs to evade their primary antiviral activity will unleash a secondary "backup" interferon response. The secondary response is sometimes called "effector-triggered immunity", a major immune strategy in plants[58] that remains poorly characterized in mammals[57,59,60].

To test the hypothesis that SP140 is an antiviral nuclear body protein, we first characterized the nature of SP140 NBs. To detect endogenously expressed SP140, we generated *HA-Sp140* knock-in mice by inserting an HA-tag after the start codon of the *Sp140* gene (Supplemental Fig. 10a). Immunoblot of BMMs from *HA-Sp140*$^{+/+}$ mice confirmed the presence of an anti-HA reactive band at the expected molecular weight of SP140 (Supplemental Fig. 10b). HA-SP140 was expressed at similar levels as WT SP140, and was functional, as assessed by its ability to repress *Ifnb1* at late timepoints in DMXAA-treated BMMs (Supplemental Fig. 10b-c). Surprisingly, immunofluorescence of *HA-Sp140*$^{+/+}$ BMMs demonstrated that SP140 forms large NBs that do not co-localize with PML bodies (Fig. 5a, Supplemental Fig. 11a). Rather, we found that SP140 NBs appeared to largely overlap with the nucleolar marker fibrillarin (Fig. 5b, Supplemental Fig. 11b).

We then tested whether SP140 has antiviral activity. We infected B6 WT and *Sp140*$^{-/-}$ BMMs with MHV68-GFP, a mouse herpesvirus engineered to encode GFP. We found that a larger fraction of *Sp140*$^{-/-}$ BMMs were infected with the virus, as assessed by GFP expression, compared to WT B6 BMMs (Fig. 5c-d, Supplemental Fig. 11c). Importantly, the effects of SP140 on viral replication were independent of the impact of SP140 on IFN-I, as *Sp140*$^{-/-}$*Ifnar*$^{-/-}$ BMMs exhibited higher levels of infection as compared to *Ifnar*$^{-/-}$ BMMs (Fig. 5c-d).

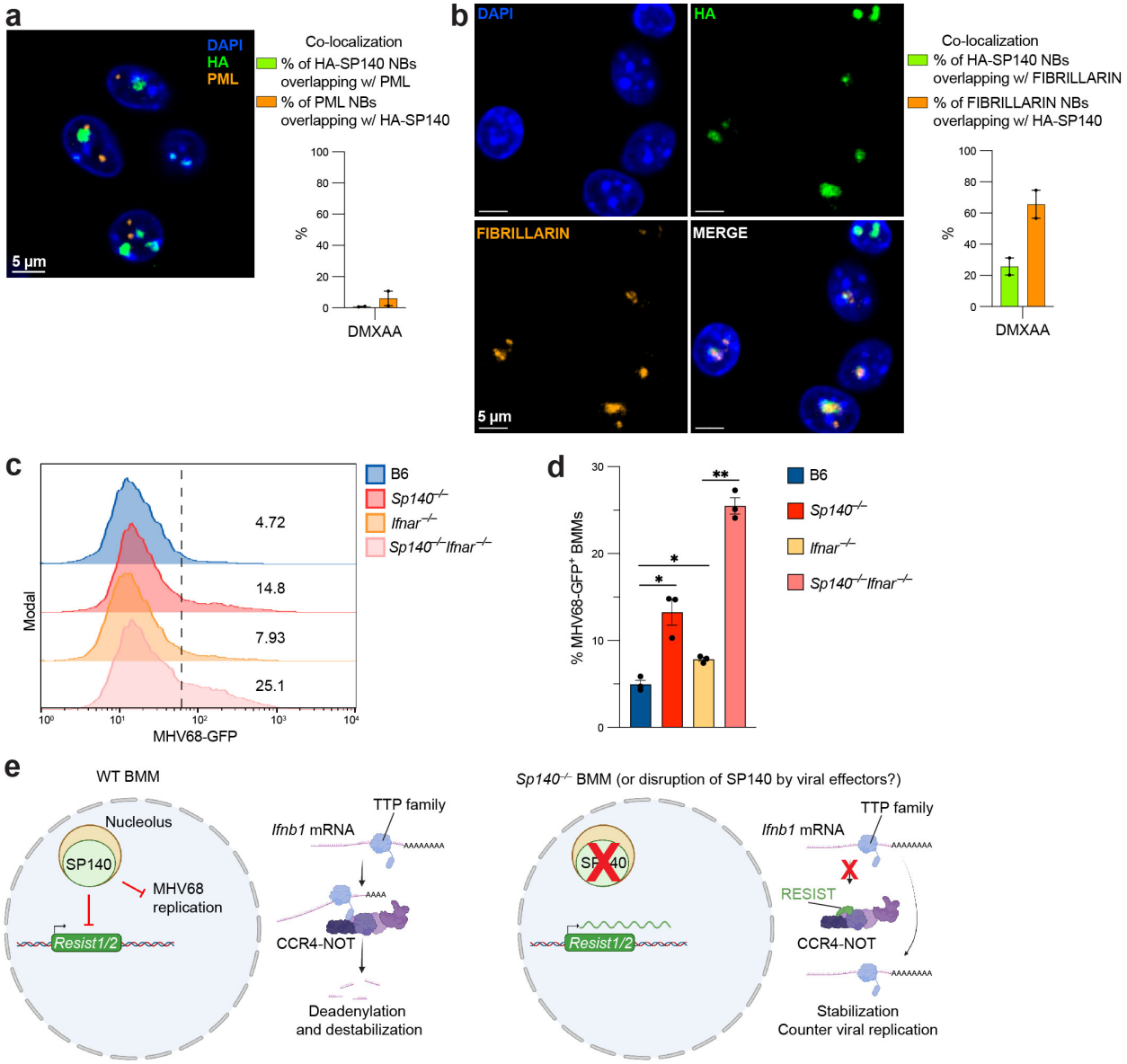

Figure 5. SP140 is an antiviral NB protein that co-localizes with nucleoli

a. Left: Immunofluorescence of *HA-Sp140*$^{+/+}$ BMMs treated with DMXAA and stained with DAPI, anti-HA, and anti-PML. Right: quantification of overlap of HA-SP140 and PML NBs for two independent experiments.
b. Immunofluorescence of *HA-Sp140*$^{+/+}$ BMMs treated with DMXAA and stained with DAPI, anti-HA, and anti-fibrillarin. Right: quantification of overlap of HA-SP140 and fibrillarin NBs for 2 independent experiments.
c. Histograms of MHV68-GFP signal in MHV68-GFP infected BMMs, assessed by flow cytometry. Numbers represent MHV68-GFP^{+} as a percentage of live cells.
d. Quantification of MHV68-GFP^{+} cells from c).
e. Schematic for the proposed model of RESIST-mediated stabilization of *Ifnb1* transcript.

Discussion

Our results describe several new findings. First, we identify RESIST as a novel positive regulator of type I IFN, which we find operates via the previously undescribed mechanism of promoting *Ifnb1* mRNA stability. Second, we demonstrate that RESIST is a direct target of SP140 transcriptional repression, and that RESIST drives the enhanced *Ifnb1* levels in *Sp140*$^{-/-}$ cells. We propose that RESIST may represent a founding example of a cytokine regulator that functions via CCR4-NOT inhibition. Third, we demonstrate that the RNA binding protein TTP (ZFP36), and its previously poorly described paralogs ZFP36L1 and ZFP36L2, are important but partly redundant negative regulators of IFN-I. Lastly, we describe an antiviral function for SP140 that is independent of its ability to regulate IFN-I. At present, the antiviral mechanism of SP140 is unknown and will be of great interest to determine in future work.

Our data support a model whereby RESIST counteracts destabilization of *Ifnb1* mRNA mediated by CCR4-NOT and the TTP-family. The activity of RESIST requires its C-terminal region. We predict that RESIST interacts through multiple binding sites with the CCR4-NOT complex. Interestingly, the predicted sites of RESIST interaction overlap with all of the known regions of interaction between CCR4-NOT and TTP. Validation of the predicted interactions between RESIST and CCR4-NOT, and a detailed investigation of whether RESIST competes with TTP family members for CCR4-NOT interaction, will require further work including the structural analyses of the RESIST-CCR4-NOT complex.

Our data do not exclude a model in which RESIST stabilizes all CCR4-NOT mRNA targets by acting as a non-specific inhibitor of deadenylation, such as RNF219[61]. However, in *Sp140*-deficient cells, we observe few upregulated transcripts besides *Resist1* and *Ifnb1* (Fig. 2a), suggesting that RESIST acts to stabilize a specific set of targets. Further work is required to determine the mechanistic basis for this specificity.

Our results highlight an important role for TTP and TTP family members ZFP36L1/ZFP36L2 in IFN-I repression in macrophages. Our finding that TTP represses IFN-I is consistent with previous work that suggests TTP negatively regulates the stability of *Ifnb1* mRNA. TTP detectably binds the 3'UTR of *Ifnb1* mRNA[47], and a hyperactive TTP mutant represses *Ifnb1* transcript levels in mouse macrophages[48]. ZFP36L1/ZFP36L2 are understudied, and genetic deletion in mice is either embryonic or perinatally lethal[62,63]. However, ZFP36L1/ZFP36L2 are known to recruit CCR4-NOT to target mRNAs[64,65] and modulate B/T cell function[65-68]. Interestingly, while *Zfp36*$^{-/-}$ mice develop severe autoinflammation, mice lacking myeloid-specific TTP expression do not develop immunopathology[69,70], suggesting functional redundancy among TTP family members in myeloid cells. Indeed, recent work described fatal autoinflammation in mice lacking myeloid-specific expression of *Zfp36/Zfp36l1/Zfp36l2*, which may result partly from elevated *Ifnb1* transcripts in these mice[71].

Our results demonstrate that SP140 largely resides in nucleoli and is intrinsically antiviral against MHV68 (Fig. 5e). In addition, we show that SP140 has evolved a secondary function: repression of the genes *Resist1/2*, which encode a previously undescribed positive regulator of IFN-I. We propose that these apparently conflicting anti- and pro-viral roles of SP140 could be explained by a host-virus arms race in the nucleus. Many viral effectors target antiviral nuclear bodies[32,52,55], but targeting of

SP140 would de-repress RESIST. RESIST would then counteract the destabilization of *Ifnb1* mRNAs mediated by the TTP family/CCR4-NOT complex, thereby augmenting IFN-I-mediated antiviral defense in response to SP140 disruption.

Finally, we speculate that the antiviral activity of SP140 could explain why multiple sclerosis and B-cell cancers are linked to LOF *SP140* mutations. Infection with MHV68-related viruses Epstein-Barr Virus (EBV) and Kaposi's sarcoma-associated herpesvirus (KSHV) are also associated with these immune disorders[72-74]. In future work, it will be of interest to determine whether individuals with LOF *SP140* mutations are more susceptible to EBV/KSHV infection, which could lead to increased risk of MS and B-cell cancers.

Methods

Mice

All animal experiments complied with the regulatory standards of, and were approved by, the University of California Berkeley Institutional Animal Care and Use Committee. Mice were maintained in specific-pathogen-free conditions with a 12-hour light/dark cycle and given water and standard chow diet (Harlan's irradiated chow) *ad libitum*. All mice were bred in-house. C57BL/6 and B6.129S2-*Ifnar1*^{tm1Agt}/Mmjax (*Ifnar*$^{-/-}$) were originally bought from Jackson laboratories and MMRC and further bred in-house. The generation and genotyping of *Sp140*$^{-/-}$ mice was previously described[29]. *HA-Sp140* knock-in mice were generated by electroporation of C57BL/6 zygotes with Cas9, Alt-R® CRISPR-Cas9 crRNA from IDT (gRNA sequence: ACUCCAAGGGACCCUGUUCA), and a homology repair Alt-R HDR donor oligo from IDT (CCCCTGAAGGAGTTCTCTCTGGGCTTCCCAGAGACTCAGAGGGGGTTCGGTCTA GTCTGAACAGGGTCCCTTGGAGTCTGTGTAGGGGATGTACCCATACGATGTTCCA GATTACGCTGCAGGAGGCTACAATGAACTCAGCAGCAGGTAAGTCCCATTCTCTCT TGTCCCTTGTCTC) as previously reported[75]. Founders were backcrossed to C57BL/6J, and mice with matching *HA-Sp140* alleles were further bred. *HA-Sp140* knock-in mice were genotyped using a qPCR-based assay from Transnetyx.

Cell culture

HEK293T and GP2 cells were obtained from the UC Berkeley Tissue Culture facility and further propagated at 37°C and 5% CO_2 in complete DMEM (10% FBS v/v (Gibco) and 1X pen-strep and glutamine (Gibco)). BlaER1 cells in B cell stage were cultured in complete RPMI, and differentiated into monocytes as described[32]. Cell lines were tested by PCR for mycoplasma (F: CACCATCTGTCACTCTGTTAACC, R: GGAGCAAACAGGATTAGATACCC) with Dreamtaq PCR reagents and validated with STR profiling by the UC Berkeley Tissue culture facility.

BMM generation and stimulation

Mice were euthanized and bones (femurs and tibias) were extracted with stringent washing in 70% ethanol. After washing in 70% ethanol and BMM media (complete RPMI with 10% MCSF (v/v) generated from 3T3 cells as described[29]), bones were crushed in a sterilized mortar and pestle and bone marrow was passed through a 70 mm filter. Bone marrow from one mouse was divided across 8 15 cm non-TC-treated

plates in 30 ml total volume in BMM media. Day of bone marrow harvest was considered as day 0, and BMMs were fed on day 3 with 10 mL media per plate. On day 6, BMMs were harvested in cold PBS by scraping and seeded on non-TC treated plates at the appropriate density (100,000 cells per non-TC 12-well and 24-well; 6-well for over 100,000 cells/well) and rested at least overnight before stimulation. To stimulate, media was aspirated and replaced with BMM containing 10 ng/mL LPS (Invivogen, tlrl-3pelps), 100 μg/mL poly(I:C) (Invivogen, tlrl-picw), or 100 μg/mL DMXAA (Cayman Chemicals, 14617).

RT-qPCR

RNA was isolated with the Omega Biotek Total RNA II kit according to kit instructions. RNA was subsequently DNAse-treated either on-column (Qiagen, 79254) or with RQ1 (Promega, M6101) according to manufacturer instructions. For BlaER1 cells, RNase-inhibitor was always included with DNase treatment (either RNaseOUT (Invitrogen) or RNasein (Promega)). RNA was then converted to cDNA with Superscript III Reverse Transcriptase (Invitrogen, 18080093) and oligo dt_{18} (NEB, S1316S) in the presence of RNase-inhibitors. Diluted cDNA was assessed by qPCR with Power SYBR™ Green PCR Master Mix (Fisher Scientific, 43-676-59) reagents, using technical duplicates. A standard curve generated from samples within each experiment was used to quantify relative amounts of transcript. *Ifnb1* transcript levels (F: GTCCTCAACTGCTCTCCACT, R: CCTGCAACCACCACTCATTC) were normalized to housekeeping genes including *Rps17* (F: CGCCATTATCCCCAGCAAG, R: TGT CGGGATCCACCTCAATG), *Oaz1* (F: GTGGTGGCCTCTACATCGAG, R: AGCAGATGAAAACGTGGTCAG), or *Hprt1* (F: GTTGGATACAGGCCAGACTTTGTTG, R: GAGGGTAGGCTGGCCTATAGGCT) as indicated in figures. Human *IFNB1* transcript quantities (F: CAGCATCTGCTGGTTGAAGA, R: CATTACCTGAAGGCCAAGGA) were normalized to *HPRT1* (F: ATCAGACTGAAGAGCTATTGTAATGA, R: TGGCTTATATCCAACACTTCGTG). DNAse-treated RNA was also included in qPCR assays to ensure complete digestion of genomic DNA. Wells with a poor ROX reference were excluded from analysis, as were samples with unusually low housekeeping gene amounts indicative of RNA degradation. Replicates in figures indicate biological replicates (separate wells).

Roadblock RT-qPCR

BMMs were either pre-treated with freshly prepared 400 μM 4-thiouridine (4SU) (Cayman Chemicals, 16373) 1-2 hours before 100 μg/mL DMXAA stimulation or treated with 4SU 2 hours after DMXAA stimulation, as previously described[30]. Briefly, RNA was harvested as described above and DNase-treated. Equal amounts of RNA (~200 ng or more) was treated with 48 μM N-ethyl maleimide (Sigma, Cat. No. 04259-5G), and quenched with 20 mM DTT. RNA was then purified with RNAClean beads (Beckman Coulter, A63987) and converted to cDNA with ProtoScript® II Reverse Transcriptase according to manufacturer instructions in the presence of RNAse inhibitors. Quantitative PCR was then performed as described above, with primers for *Ifnb1* (F: TGGATGGCAAAGGCAGTGTAA, R: CACCTACAGGGCGGACTTC) and *Rps17* (see above). In some experiments, house-keeping normalized *Ifnb1* is displayed in figures as the percentage of average *Ifnb1/Rps17* quantity present at 2 hours of DMXAA

stimulation for each condition. To validate the Roadblock RT-qPCR protocol, in every Roadblock RT-qPCR experiment, BMMS were also pre-treated in parallel with 4SU before DMXAA treatment, and RNA was isolated at T=2 and other timepoints indicated in figures and converted to cDNA. NEM treatment was confirmed to reduce detection of *Ifnb1* transcript by qPCR ~10-fold with 4SU pre-treatment before DMXAA for every Roadblock RT-qPCR experiment.

RNA-seq sample generation and analysis

Day 6 BMMs derived from B6 and *Sp140*$^{-/-}$, or *Ifnar*$^{-/-}$ and *Sp140*$^{-/-}$*Ifnar*$^{-/-}$ mice were seeded at 1 e6/well in 6 well non-TC plates and rested overnight. BMMs were then either left unstimulated or stimulated with DMXAA (100 μg/mL for B6 and *Sp140*$^{-/-}$ BMMs, and 10 μg/mL DMXAA for *Ifnar*$^{-/-}$ and *Sp140*$^{-/-}$*Ifnar*$^{-/-}$ BMMs) for either 8 hours for B6 and *Sp140*$^{-/-}$ BMMs, or 4 hours for *Ifnar*$^{-/-}$ and *Sp140*$^{-/-}$*Ifnar*$^{-/-}$ BMMs. RNA was isolated with the Omega Biotek Total RNA II kit, and DNAse-treated with TURBO DNAse (ThermoFisher Scientific, AM2238) according to manufacturer instructions. For RNA from B6 and *Sp140*$^{-/-}$ BMMs, single-index libraries were generated by Azenta, using rRNA depletion (Qiagen, QIAseq FastSelect – HMR rRNA Removal kit) and the NEBNext RNA Ultra kit (NEB). Libraries were evenly split across 2 lanes of an Illumina Hiseq flow cell and sequenced (150 bp paired-end reads, depth of 25-30M reads/sample). For *Ifnar*$^{-/-}$ and *Sp140*$^{-/-}$*Ifnar*$^{-/-}$ BMM samples, libraries were prepared for Illumina sequencing with dual indices using polyA selection and KAPA HyperPrep reagents (Roche) after heat fragmentation through the UC Berkeley QB3 Vincent J. Coates Genomics Sequencing Laboratory. Libraries were subsequently size selected between 450-500 bp, and then sequenced on an Illumina Novaseq flow cell for a depth of over 20M mapped reads (150 bp, paired-end). B6 and *Sp140*$^{-/-}$ samples were collected separately from *Ifnar*$^{-/-}$and *Sp140*$^{-/-}$*Ifnar*$^{-/-}$ samples. Three biological replicates for each genotype and condition were collected across three independent experiments from 3 separate mice for each genotype. Adapters and low-quality reads were trimmed using BBDuk v38.05 with arguments 'ktrim=r k=23 mink=11 hdist=1 mapq=10 qtrim=r trimq=10 tpe tbo'. For UCSC genome browser visualization, reads were mapped to mm10 using hisat2 v2.1.0 with options '--no-softclip -k 100 | samtools view -q 10 -Sb - | samtools sort'. CPM normalized bigwigs were made using deepTools bamCoverage v3.0.1. For transcript quantification, reads were mapped to mm10 (gencode.vM18.annotation.gtf) using using Salmon v0.13.1 with options '--libType A --validateMappings --rangeFactorizationBins 4 --gcBias'. Differentially expressed genes were called using DESeq2 v1.38.3 with design '~batch + genotype + treatment + genotype:treatment'. For differential expression analysis of *Sp140*$^{-/-}$ vs. B6 BMMs and *Sp140*$^{-/-}$*Ifnar*$^{-/-}$ vs. *Ifnar*$^{-/-}$ BMMs, normalized count data was derived from the following DESeq2 comparisons: 1) SP140-deficient BMMs treated with DMXAA (3 replicates) vs. SP140-WT BMMs treated with DMXAA (3 replicates); and 2) untreated SP140-deficient BMMs (3 replicates) vs. untreated SP140-WT BMMs (3 replicates). Genes with zero counts across all samples were removed. Volcano plots were generated with ggplot2 v3.5.0 R package.

ATAC-seq sample generation and analysis

B6 and *Sp140*$^{-/-}$ samples BMMs were derived and stimulated as described above with 100 μg/mL DMXAA for 8 hours in three separate experiments, in parallel to samples generated for RNA-seq. BMMs were harvested in PBS and counted, and ATAC-seq samples were generated from 100,000 input cells essentially as described[76], except that isolated nuclei were spun at 1000 *x g*. Illumina-compatible libraries were prepared as described[76], with additional Ampure XP bead (Beckman Coulter) purification to remove contaminating adaptor dimers. Samples were sequenced with Azenta on an Illumina HiSeq flow cell (over 50M paired end reads/sample, 150 bp reads). Adapters and low quality reads were trimmed using BBDuk v38.05 with arguments 'ktrim=r k=23 mink=11 hdist=1 maq=10 qtrim=r trimq=10 tpe tbo' and mapped to mm10 using BWA-MEM v0.7.15, and only uniquely mapping reads with a minimum MAPQ of 10 were retained. Fragments aligning to the mitochondrial genome were removed. Peak calling was performed using complete and size subsetted alignment files with MACS2 v2.1.1 with paired-end options '--format BAMPE --SPMR -B --broad'. For visualization, CPM normalized bigwigs were made using deepTools bamCoverage v3.0.1.

BMM transduction

Low passage HEK293T cells or GP2s were seeded in a 6-well format on tissue culture treated plates and rested at least overnight. To generate lentivirus, HEK293Ts at >70% confluency in a 6-well TC-treated plate were transfected with 0.468 μg VSV-G (pMD2.G, Addgene plasmid #12259), 1.17 μg D8.9 packaging vector, and 1.56 μg of doxycycline-inducible, puromycin-selectable lentiviral vector per well using Lipofectamine 2000 according to manufacturer instructions. The lentiviral backbone used in this study (pLIP) was adapted from pLIX (Addgene #41394) by removal of ccdB[32] . Gene blocks encoding codon-optimized mouse/human RESIST, or mCherry were cloned into pLIP after the dox-inducible promoter, digested with NheI and BamHI, with Infusion reagents (Takara), essentially as described[32]. RESISTΔC constructs were also generated by PCR to remove residues after D161 followed by Infusion cloning into the pLIP backbone. To generate retrovirus, GP2s at > 70% confluency in a 6-well plate were transfected with 0.5 μg of VSV-G and 3.5 μg of retroviral vector per well with Lipofectamine 2000. Retroviral vectors in this study (SINV HA-SP140, SINV-SP140) were derived from the self-inactivating retrovirus pTGMP (Addgene plasmid #32716, from the lab of Scott Lowe). Mouse SP140 or HA-SP140 codon-optimized cDNA was cloned into pTGMP with Infusion (Takara), modified to include a minimal CMV promoter driving SP140 constructs, followed by a PGK promoter driving a puromycin resistance cassette. Eighteen-20 hours after transfection, media on transfected cells was changed to 1 mL BMM media. Bone marrow was harvested as described above, and plated in BMM media without dilution. Retronectin (Takara) treated 6-well plates were generated according to manufacturer instructions. The following day (~30 hours after changing media on transfected cells), virus was harvested from transfected cells by filtration of supernatant through a 0.45 μm filter and added to 1 e6/well of bone marrow in 4 mL total of BMM media. Plates were spun at 650 *x g* for 1.5-2 hours at 37°C. Three days after bone marrow harvest, BMMs were fed with 1.33 mL BMM media. BMMs were puromycin-selected on day 4 after BMM harvest with 2.75-5 μg/mL puromycin. Puromycin kill curves were determined for every stock to identify the lowest concentration needed for BMM selection, and a non-transduced well or BMMs

transduced with a retroviral vector lacking a puromycin resistance cassette were used to verify complete killing of non-transduced cells by puromycin. After puromycin selection (2 days), media was exchanged and BMMs were allowed to recover for 2-6 days before seeding. BMMs lentivirally transduced with pLIP constructs were pre-treated overnight-24 hours with 2.5 μg/mL doxycycline, then restimulated with 100 μg/mL DMXAA and fresh doxycycline. Cells were harvested at timepoints indicated in the figure legends for either RNA isolation or co-immunoprecipitation.

HA-SP140 CUT&RUN and analysis

Sp140$^{-/-}$ BMMs were retrovirally transduced with HA-SP140 or SP140 as described above, and stimulated for 8 hours with 100 μg/mL DMXAA. Half a million cells were input into CUT&RUN in biological triplicates using the Epicypher CUTANA™ ChIC/CUT&RUN kit (Epicypher, 14-1048, v3), using 0.5 μg of rabbit anti-HA monoclonal antibody (Cell Signaling Technologies, C29F4) with *E. coli* genomic DNA spike-in. Non-transduced B6 BMMs (0.5 e6) were also put into CUT&RUN with 0.5 μg of rabbit isotype control IgG (Epicypher, 13-0042), with a single biological replicate. CUT&RUN was carried out on isolated nuclei according to kit instructions. Libraries were prepared using the Epicypher CUTANA™ CUT&RUN library prep kit (Epicypher, 14-1001) according to kit instructions, then sequenced on an Illumina Novaseq flow cell with 250 bp paired-end reads for ~6 million reads per sample. Adapters and low-quality reads were trimmed using BBDuk v38.05 using options 'ktrim=r k=23 mink=11 hdist=1 maq=10 tpe tbo qtrim=r trimq=10'. Trimmed reads were aligned to the mm10 assembly using BWA-MEM v0.7.15, and only uniquely mapping reads with a minimum MAPQ of 10 were retained. Fragments aligning to the mitochondrial genome were removed. Peak calling was performed using complete and size subsetted alignment files with MACS2 v2.1.1 with paired-end options '--format BAMPE --pvalue 0.01 --SPMR -B --call-summits'. Bigwig files were prepared from the MACS2 normalized bedgraph files using bedGraphToBigWig v4. MACS2 peak scores, the normalized number of sequence reads that originate from a bound genomic location, were output for HA-SP140 peaks.

Cistrome and GREAT analysis

Replicate MACS2 CUT&RUN peak files were merged, then controls (IgG and SP140) were subtracted from the HA-SP140 peak file using bedtools intersect (v2.28.0)[77] to output a file of SP140 peaks. This SP140 peak file was used as input in the cistrome toolkit data browser (http://dbtoolkit.cistrome.org/) looking for significant binding overlap of histone marks and variants in mm10. The SP140 peak file was also used as input for Genomic Regions Enrichment of Annotations Tool (GREAT)[78].

Recombinant protein expression and purification

A SUMO-tagged fragment of ANXA2R (residues 1–160) was produced in E. coli BL21 (DE3) Star cells (Thermo Fisher Scientific) in LB medium at 20 °C as a fusion protein carrying an N-terminal His6-SUMO tag and two C-terminal StrepII tags. Cells were resuspended in lysis buffer (50 mM HEPES, 500 mM NaCl, 25 mM Imidazole, pH 7.5) and lysed using a Branson Ultrasonics Sonifier SFX550. The lysate was cleared by centrifugation at 40,000 × *g* for 1 hr at 4 °C. The cleared lysate was loaded onto a 5 ml HisTrap column (Cytiva). The bound protein was eluted over a linear gradient with

elution buffer (50 mM HEPES, 200 mM NaCl, 500 mM Imidazole, pH 7.5). The final step was size exclusion chromatography on a Superdex 200 26/600 column in a buffer containing 10 mM HEPES, 200 mM NaCl, 2 mM DTT, pH 7.5. In addition, a fusion protein of ANXA2-S100A was produced and purified in the same manner.

StrepTactin pull-down assay

StrepII-tagged MBP, as well as StrepII-tagged and SUMO-tagged SUMO-SMARCA3 (residues 26-39) were produced in E. coli BL21 (DE3) Star cells (Thermo Fisher Scientific) grown in auto-induction medium overnight at 37 °C. Cells were resuspended in lysis buffer (50 mM HEPES, 500 mM NaCl, pH 7.5) and lysed using a Branson Ultrasonics Sonifier SFX550, the lysate was then cleared by centrifugation at 40,000 × *g* for 1 hr at 4 °C. The cleared lysate or purified ANXA2R was incubated with StrepTactin Sepharose resin (Cytiva, 28935599). After a 1-hr incubation beads were washed twice with 50 mM HEPES, 500 mM NaCl, pH 7.5, 0.03% Tween, once with 50 mM HEPES, 500 mM NaCl, pH 7.5, and once with binding buffer (50 mM HEPES, 200 mM NaCl, pH 7.5). Purified ANXA2-S100A was added to the bead-bound proteins. After a 1-h incubation, beads were washed four times with binding buffer and proteins were eluted with 50 mM biotin in binding buffer. The eluted proteins were analyzed by SDS-polyacrylamide gel electrophoresis followed by Coomassie blue staining.

BlaER1 transduction and stimulation

Lentivirus was generated from HEK293T cells transfected with pLIP constructs (either mCherry or human RESIST either untagged or with N/C-terminal HA tags) as described for BMM transduction above. Virus was overlaid onto BlaER1 cells, which were subsequently puromycin selected and differentiated as described[32]. After 5 days of differentiation, BlaER1 cells were stimulated with 2.5 μg/mL doxycycline and fresh cytokines overnight. Media with new cytokines, fresh doxycycline, and ADU-S100 at a final concentration of 5 μg/mL (Aduro) was added the next day. At indicated timepoints, adherent and non-adherent cells were harvested and either lysed in TRK lysis buffer (Omega Biotek Total RNA kit) for RNA isolation or prepared for co-immunoprecipitation (below). RNA was isolated as quickly as possible from lysates as described above, and converted to cDNA with Superscript reagents and RNAse-inhibitors as described above.

Co-immunoprecipitation

BlaER1 monocytes or BMMs were transduced with RESIST constructs or mCherry and treated with doxycycline, followed by DMXAA treatment of BMMS or ADUS-100 treatment of BlaER1s, as described above. Cells (0.6 e6 – 2.4 e6) were harvested at timepoints indicated in figure legends, and lysed on ice in 300-600 mL lysis buffer (50 mM Tris-HCl pH 7.5, 0.2% NP-40, 5% glycerol, 100 mM NaCl, 1.5 mM $MgCl_2$, 1X protease inhibitor cocktail) for 30 minutes. Lysate was clarified by centrifugation at 18213 *x g* for 30 minutes at 4°C and quantified by BCA to ensure approximately equal amounts of input protein. One tenth of clarified lysate was diluted in Laemmli buffer for input sample. Supernatant was incubated with anti-HA magnetic beads (ThermoFisher, 88836) rotating 3 hrs – ON at 4°C. Beads with lysate were then washed three times with lysis buffer (1 mL per wash), then immunoprecipitated proteins were eluted in 30-50 mL

Laemmli buffer by boiling for 5 minutes. Samples were then analyzed by immunoblot.

Immunoblot

Samples diluted in Laemmli buffer were run on 4-12% Bis-Tris protein gels (Invitrogen) and then transferred to PVDF membranes at 35 volts for 90 minutes. Membranes were blocked in either Odyssey Licor PBS blocking buffer or in 2-5% non-fat dry milk diluted in TBST. Membranes were then probed with antibodies at 4°C overnight diluted in 5% BSA TBST. Antibodies used in this study were rat anti-HA (Roche, clone 3F10, 1186742300, 1:1000), mouse anti-actin (Santa Cruz Biotechnology, sc-4478, 1:1000), rabbit anti-CNOT1 (Cell Signaling Technologies, 44613S, 1:1000), rabbit anti-CNOT9 (Proteintech, 22503-1-AP, 1:500), rabbit anti-TTP (Millipore Sigma, ABE285, 1:1000), rabbit anti-CNOT11 (Sigma Aldrich, HPA069823, 0.4 μg/mL), rabbit anti-ZFP36L1 (Cell Signaling Technologies, 30894S, 1:1000), rabbit anti-ZFP36L2 (Abcam, ab70775, 1:1000), and rabbit-SP140 (Covance, as previously described[29]; 1:1000).

AlphaFold structure predictions

AlphaFold-Multimer v2.3.2[43] was run on equipment hosted by the Cal Cryo EM facility comprised of an Nvidia GPU and >72 TB of storage space. Mouse RESIST and CCR4-NOT amino acid sequences were from NCBI (RESIST: XP_006517870.1; CNOT1 M-HEAT: XP_036009857.1, with a start codon followed by residues 815-1007; CNOT11: NP_082319.1; CNOT1 N-MIF4G:, XP_036009857.1, residues 1-695; CNOT10: NP_705813.2; CNOT9: NP_067358.1). Briefly, Alphafold was run in multimer mode on RESIST with CNOT1 M-HEAT, CNOT9, or CNOT1 N-MIF4G/CNOT10/CNOT11 with default settings and max template date specified as 2023-01-01, and *--db_preset=full_dbs.* Output models were visualized in ChimeraX (1.6.1), and aligned using the matchmaker command. PAE plots and structures colored by pLDDT were visualized with PAEViewer[79].

Gene disruption in BMMs with Cas9:gRNA electroporation

BMMs were harvested in PBS and electroporated with Cas9 2 NLS nuclease (Synthego) complexed with gRNAs (Synthego, sgRNA EZ kits), and Alt-R® Cas9 Electroporation Enhancer (IDT, 1075916), in Lonza P3 buffer (Lonza, V4XP-3032) with buffer supplement as described[42]. Electroporation was performed with a Lonza 4D-Nucleofector Core Unit (AAF-1002B) using the program CM-137. Electroporated BMMs were immediately plated in BMM media. A half-media exchange was performed every 2 days until day 10 after bone marrow harvest, when BMMs were seeded for downstream assays. Human BlaER1 cells transduced with RESIST constructs or mCherry were similarly electroporated, and cultured in complete RPMI. Knockout efficiency was evaluated by immunoblot or by PCR of genomic DNA for targeted regions followed by ICE analysis (Synthego) as indicated in figure legends. *Gm21188* (*Resist1*) was genotyped with Primestar PCR reagents and primers F1: ATTGAGAAATCCGTTTGTAATGGG and R1: TAGGCGAATTTCGTGGCACA according to manufacturer instructions with an annealing temperature of 55°C, or using Q5 PCR reagents and primers F2: TTGAGAAATCCGTTTGTAATGGG, R2: GCCTTTCTCCGGATTCACGA, with cycling conditions: 98°C 3 min, 35 cycles of 98°C 10 s, 63.5°C 20 s, 72°C 1:05 min. *Gm36079* (*Resist2*) was genotyped with F:

TGGTATTCTCTAGAGATAACATCACAGCACCTACTTACTCC, R: CCTCCCCTCGCCATCACTGCCTG, using Phusion GC PCR reagents and cycling conditions of: 98°C 30 s, then 30-35 cycles of 98°C for 10 s, 72°C for 15 s, 72°C for 1 min. Disruption of *Rc3h1* was determined by PCR (F: CACACTATGTGCTGACTGTATCTACAGAAG, R: TCCCCTCAGGTAAAACAGTGC, cycling: 98°C 30 s, then 30 cycles of 98°C 10 s, 60°C 5 s, 72°C 1 min) with Phusion GC PCR reagents. Disruption of *Rc3h2* was determined by PCR (Q5 PCR reagents with F2: AGGGCATAAGATGTTGCACAGA, R2: ACTGCTAACCCGAGCATCAG: and cycling of 98°C 3 min, then 35 cycles of 98°C 10 s, 60°C 20 s, 72°C 40 s). PCRs were cleaned by gel extraction, Ampure XP beads (Beckman Coulter), or treatment with FAST-AP and ExoI before submission for Sanger sequencing. Guide RNA sequences used in this study were:
Gm21188/Gm36079 gRNA 1: GCUGGGCCUCUUGCACCAGA
Gm21188/Gm36079 gRNA 2: CGACGAUGGCGGUGACUACC
Cnot1 gRNA 1: UGUGAAUCGGCACGGUCCUG
Cnot1 gRNA 2: ACUCAUUCAGGAUUAACAGA
Cnot11 gRNA 1: UCCAUCAAGGCAAUCUGGCG
Cnot11 gRNA 2: GCUGAGCAUCAUCUCGGAGG
Cnot9 gRNA 1: CAUUGCAAACUCUGUUAGAC
Cnot9 gRNA 2: GCCUACUGCACUAGCCCAAG
Human *CNOT9* gRNA 1: GCCUACUACACUGGCACAAG
Human *CNOT9* gRNA 2: GACUGGUGUGCUGUCAAGGU
Zfp36 gRNA 1: CAUGACCUGUCAUCCGACCA
Zfp36 gRNA 2: CUUCAUCCACAACCCCACCG
Zfp36l1 gRNA 1: AAAAAUGGUGGCGGACACGA
Zfp36l1 gRNA 2: ACGGGCAAAAGCCGAUGGTG
Zfp36l2 gRNA 1: CAAGAAGUCGAUAUCGUAGA
Zfp36l2 gRNA 2: GAGAGCGGCACGUGCAAGUA
Rc3h1 gRNA: CAAAUGGGCAAGCCUUACGG
Rc3h2 gRNA: UCGGUGAAGUUUAUUCAAGC

MHV68-GFP infection
Day 7 BMMs were generated as described above, and 250,000 cells were infected with MHV68-GFP at a multiplicity of infection (MOI) of ~3 for 3-4 hours in serum-free RPMI supplemented with pen/strep and glutamine. MHV68-GFP was a gift of Laurent Coscoy, UC Berkeley, and Britt Glaunsinger, UC Berkeley. MHV68-GFP titer was estimated by infection of 3T3 cells, and calculated by the assumption that a viral dilution resulting in 100% of infected 3T3 cells corresponds to an approximate MOI of 5. After infection, media was replaced and BMMs were cultured for an additional 20-24 hours before cells were harvested in PBS, stained with Ghost Dye Far Red 780, fixed with the BD Cytofix Cytoperm kit according to kit instructions, then washed and analyzed by flow cytometry. Data were analyzed with FlowJo.

Immunofluorescence (IF) microscopy
BMMs were seeded on glass coverslips between 0.5 e6 – 1 e6/slip in BMM media lacking antibiotics and rested overnight. BMMs were stimulated with 100 μg/mL DMXAA

for 8 hours, fixed in 4% freshly prepared paraformaldehyde (Electron Microscopy Sciences) for 10 minutes at room temperature, then permeabilized in freshly made 0.2% Triton X-100 and 0.2% BSA in PBS on ice for 10 minutes. Coverslips were washed 3 times with PBS and then blocked in goat serum and FC-block (TruStain FcX™ PLUS, anti-mouse CD16/32) for one hour, then incubated overnight at 4°C in primary antibody diluted in PBS with 1% Tween-20 and 1% BSA. Primary antibodies and dilutions were mouse anti-PML Millipore Sigma, 05-718, 1:100; rat anti-HA, Roche, 11867423001, 1:200; rabbit anti-Fibrillarin, Abcam, ab166630 1:100. Coverslips were washed 3 times in PBS, then incubated in secondary antibody diluted 1:1000 in PBS with 1% Tween-20 and 1% BSA for 2-3 hours at room temperature. Secondary antibodies used were donkey anti-rat Alexa Fluor 488, Invitrogen, A21208; goat anti-mouse Alexa Fluor 647, Invitrogen, A21236; goat anti rabbit 647, Life technologies, A21244. After 3 PBS washes of coverslips, nuclei were stained with DAPI at 1 μg/mL in PBS for 10 minutes at room temperature. Coverslips were mounted in Vectashield mounting medium (Vector Laboratories, H-1000-10). Coverslip edges were then sealed with clear nail polish before imaging on a Zeiss LSM 880 NLO AxioExaminer at 63x magnification.

IF image processing and quantification

For independent experiments as indicated in figure legends, Z stacks were processed by Imaris File Converter v10.0.1 followed by Imaris Stitcher v9.9.1. Images were Gaussian filtered (0.132 mm) and screenshots were generated for figures. Surfaces for DAPI, HA-SP140, PML, and fibrillarin were generated in Imaris using split-touching of 1 mm for HA-SP140, PML, and fibrillarin surfaces and 5 mm for DAPI surfaces. Surface statistics were then exported. Surfaces were first filtered as DAPI+ (within 2 standard deviations below average fluorescence intensity of DAPI surfaces), then filtered by size (over 0.2 mm^3). HA-SP140 nuclear bodies were considered to overlap fibrillarin if fibrillarin intensity mean for an HA-SP140 surface was within 2 standard deviations of average fluorescence intensity for fibrillarin surfaces, and vice versa for fibrillarin surfaces overlapping with HA-SP140 surfaces. The same criteria for overlap was applied to HA-SP140 and PML surfaces. Mean fluorescence intensities of surfaces were calculated for over 100 nuclei for each independent experiment.

Statistical analysis and schematics

All results except HA-SP140 CUT&RUN and AlphaFold predictions were repeated at least twice in independent experiments. Statistics and graphs for RT-qPCR experiments and MHV68-GFP infections were generated using GraphPad Prism. For these data, which were assumed to be normally distributed, * = $p < 0.05$, ** = $p < 0.005$, ns = not significant, calculated with a two-tailed t-test using Welch's correction. The mean for this data was graphed, and replicates are individually represented by dots. Error bars indicate standard error. Data shown in each figure represent the source data. Replicates in RT-qPCR or MHV68 infections represent separate wells within an experiment. Schematics were generated in Biorender.

Data availability

HA-SP140 anti-HA CUT&RUN data is available at GEO accession: GSE269315. RNA-seq for for *Ifnar*$^{-/-}$ and *Sp140*$^{-/-}$*Ifnar*$^{-/-}$ BMMs is available at GEO accession:

GSE269761. RNA-seq and ATAC-seq for B6 and *Sp140*$^{-/-}$ BMMs is available at GEO accession GSE269808 and GSE269811 respectively.

Source code
Source code for all analysis scripts and pipelines is available at https://github.com/adziulko/The-SP140-RESIST-pathway.

Author contributions
Conceptualization: K.W. and R.E.V. Data analysis: K.W., A.D., J.A., P.A., A.C, E.C. Investigation: K.W., A.D., J.A., O.V.L., D.T., A.C., R.C., D.K., P.A., L.C., E.C., R.E.V. Writing: K.W., A.D., and R.E.V. Resources: A.L., H.D. A.Y.L., B.G., L.C., G.L. Funding acquisition: R.E.V.

Acknowledgements
We thank the Vance and Barton labs for input and advice, and thank Ella Brydon for technical assistance. We thank Dr. Jessie Li (UC Davis Bioinformatics) for preliminary analysis of ATAC-seq and CUT&RUN datasets. We also thank Eugene Valkov for supporting DT and for comments on the manuscript. R.E.V. is an Investigator of the Howard Hughes Medical Institute, and research in his lab is supported by NIH grants AI075039, AI063302, and AI155634. DT was supported by the Intramural Research Program of the National Institutes of Health.

Competing Interests
R.E.V. consults for Tempest Therapeutics and X-biotix.

References
1 Crowl, J. T., Gray, E. E., Pestal, K., Volkman, H. & Stetson, D. B. Intracellular Nucleic Acid Detection in Autoimmunity. *Annual Review of Immunology* **35** (2017). https://doi.org/10.1146/annurev-immunol-051116-052331
2 Borden, E. C. Interferons α and β in cancer: therapeutic opportunities from new insights. *Nature Reviews Drug Discovery* **18** (2019). https://doi.org/10.1038/s41573-018-0011-2
3 Schoggins, J. W. Interferon-Stimulated Genes: What Do They All Do? *Annual Review of Virology* **6**, 567-584 (2019). https://doi.org/10.1146/annurev-virology-092818-015756
4 Sarkar, S. N., Harioudh, M. K., Shao, L., Perez, J. & Ghosh, A. The Many Faces of Oligoadenylate Synthetases. *Journal of Interferon & Cytokine Research* **43** (2023). https://doi.org/10.1089/jir.2023.0098
5 Tan, X., Sun, L., Chen, J. & Chen, Z. J. Detection of Microbial Infections Through Innate Immune Sensing of Nucleic Acids. *Annual Review of Microbiology* **72**, 447-478 (2018). https://doi.org/10.1146/annurev-micro-102215-095605
6 McNab, F. *et al.* Type I interferons in infectious disease. *Nature Reviews Immunology* **15** (2015). https://doi.org/10.1038/nri3787
7 Whittemore, L. A. & Maniatis, T. Postinduction turnoff of beta-interferon gene expression. *Molecular and cellular biology* **10**, 1329-1337 (1990).

8 Akira, S. & Maeda, K. Control of RNA Stability in Immunity. *Annual Review of immunology* **39**, 481-509 (2021). https://doi.org/10.1146/annurev-immunol-101819-075147
9 Gokhale, N. S., Smith, J. R., Gelder, R. D. V. & Savan, R. RNA regulatory mechanisms that control antiviral innate immunity. *Immunological Reviews* **304** (2021). https://doi.org/10.1111/imr.13019
10 Fernandez-Ruiz, R. & Niewold, T. B. Type I Interferons in Autoimmunity. *Journal of Investigative Dermatology* **142**, 793-803 (2022). https://doi.org/10.1016/j.jid.2021.11.031
11 Fraschilla, I. & Jeffrey, K. L. The Speckled Protein (SP) Family: Immunity's Chromatin Readers. *Trends in Immunology* **41**, 572-585 (2020). https://doi.org/10.1016/j.it.2020.04.007
12 Ferguson, B. J. *et al.* AIRE's CARD revealed, a new structure for central tolerance provokes transcriptional plasticity. *Journal of Biological Chemistry* **283**, 1723-1731 (2008). https://doi.org/10.1074/jbc.M707211200
13 Halonen, M. *et al.* APECED-causing mutations in AIRE reveal the functional domains of the protein. *Human Mutation* **23**, 245-257 (2004). https://doi.org/10.1002/humu.20003
14 Staněk, D. & Fox, A. H. Nuclear bodies: news insights into structure and function. *Current Opinion in Cell Biology* **46**, 94-101 (2017). https://doi.org/10.1016/j.ceb.2017.05.001
15 Bhattacharya, B. *et al.* The integrated stress response mediates necrosis in murine Mycobacterium tuberculosis granulomas. *Journal of Clinical Investigation* **131** (2021). https://doi.org/10.1172/JCI130319
16 Amatullah, H. *et al.* Epigenetic reader SP140 loss of function drives Crohn's disease due to uncontrolled macrophage topoisomerases. *Cell* **185**, 3232-3247 e3218 (2022). https://doi.org/10.1016/j.cell.2022.06.048
17 Mehta, S. *et al.* Maintenance of macrophage transcriptional programs and intestinal homeostasis by epigenetic reader SP140. *Science immunology* **2** (2017). https://doi.org/10.1126/sciimmunol.aag3160
18 Fraschilla, I., Amatullah, H., Rahman, R.-U. & Jeffrey, K. L. Immune chromatin reader SP140 regulates microbiota and risk for inflammatory bowel disease. *Cell Host & Microbe* **30**, 1370-1381.e1375 (2022). https://doi.org/10.1016/j.chom.2022.08.018
19 Karaky, M. *et al.* SP140 regulates the expression of immune-related genes associated with multiple sclerosis and other autoimmune diseases by NF-κB inhibition. *Human Molecular Genetics* **27**, 4012-4023 (2018). https://doi.org/10.1093/hmg/ddy284
20 Ghiboub, M. *et al.* Modulation of macrophage inflammatory function through selective inhibition of the epigenetic reader protein SP140. *BMC Biology* **20** (2022). https://doi.org/10.1186/s12915-022-01380-6
21 Tanagala, K. K. K. *et al.* SP140 inhibits STAT1 signaling, induces IFN-γ in tumor-associated macrophages, and is a predictive biomarker of immunotherapy

response. *Journal for Immunotherapy of Cancer* **10** (2022). https://doi.org/10.1136/jitc-2022-005088

22 Sumida, T. S. *et al.* Type I interferon transcriptional network regulates expression of coinhibitory receptors in human T cells. *Nature Immunology* **23** (2022). https://doi.org/10.1038/s41590-022-01152-y

23 Matesanz, F. *et al.* A functional variant that affects exon-skipping and protein expression of *SP140* as genetic mechanism predisposing to multiple sclerosis. *Human Molecular Genetics* **24**, 5619-5627 (2015). https://doi.org/10.1093/hmg/ddv256

24 Di Bernardo, M. C. *et al.* A genome-wide association study identifies six susceptibility loci for chronic lymphocytic leukemia. *Nature Genetics* **40**, 1204-1210 (2008). https://doi.org/10.1038/ng.219

25 Franke, A. *et al.* Genome-wide meta-analysis increases to 71 the number of confirmed Crohn's disease susceptibility loci. *Nature genetics* **42**, 1118-1125 (2010). https://doi.org/10.1038/ng.717

26 Jostins, L. *et al.* Host-microbe interactions have shaped the genetic architecture of inflammatory bowel disease. *Nature* **491**, 119-124 (2012). https://doi.org/10.1038/nature11582

27 Yi, S. *et al.* Genomic and transcriptomic profiling reveals distinct molecular subsets associated with outcomes in mantle cell lymphoma. *Journal of Clinical Investigation* **132** (2022). https://doi.org/10.1172/jci153283

28 Sawcer, S. *et al.* Genetic risk and a primary role for cell-mediated immune mechanisms in multiple sclerosis. *Nature 2011 476:7359* **476** (2011). https://doi.org/10.1038/nature10251

29 Ji, D. X. *et al.* Role of the transcriptional regulator SP140 in resistance to bacterial infections via repression of type I interferons. *Elife* **10** (2021). https://doi.org/10.7554/eLife.67290

30 Watson, M. J. & Thoreen, C. C. Measuring mRNA Decay with Roadblock-qPCR. *Current Protocols* **2** (2022). https://doi.org/10.1002/cpz1.344

31 Skene, P. J. & Henikoff, S. An efficient targeted nuclease strategy for high-resolution mapping of DNA binding sites. *Elife* **6** (2017). https://doi.org/10.7554/eLife.21856

32 Gaidt, M. M. *et al.* Self-guarding of MORC3 enables virulence factor-triggered immunity. *Nature* **600**, 138-142 (2021). https://doi.org/10.1038/s41586-021-04054-5

33 Assouvie, A. *et al.* A genetic variant controls interferon-β gene expression in human myeloid cells by preventing C/EBP-β binding on a conserved enhancer. *PLOS Genetics* **16**, e1009090 (2020). https://doi.org/10.1371/journal.pgen.1009090

34 Ferri, F. *et al.* TRIM33 switches off Ifnb1 gene transcription during the late phase of macrophage activation. *Nature Communications* **6**, 8900-8900 (2015). https://doi.org/10.1038/ncomms9900

35 Decque, A. *et al.* Sumoylation coordinates the repression of inflammatory and anti-viral gene-expression programs during innate sensing. *Nature Immunology* **17**, 140-149 (2016). https://doi.org/10.1038/ni.3342
36 Lu, G. *et al.* Cloning and Characterization of the Annexin II Receptor on Human Marrow Stromal Cells. *Journal of Biological Chemistry* **281**, 30542-30550 (2006). https://doi.org/10.1074/jbc.m607072200
37 Hallgren, J. *et al.* DeepTMHMM predicts alpha and beta transmembrane proteins using deep neural networks. *bioRxiv* (2022). https://doi.org/10.1101/2022.04.08.487609
38 Hubel, P. *et al.* A protein-interaction network of interferon-stimulated genes extends the innate immune system landscape. *Nature Immunology* **20**, 493-502 (2019). https://doi.org/10.1038/s41590-019-0323-3
39 Oh, Y.-S. *et al.* SMARCA3, a Chromatin-Remodeling Factor, Is Required for p11-Dependent Antidepressant Action. *Cell* **152** (2013). https://doi.org/10.1016/j.cell.2013.01.014
40 Raisch, T. & Valkov, E. Regulation of the multisubunit CCR4-NOT deadenylase in the initiation of mRNA degradation. *Current Opinion in Structural Biology* **77** (2022). https://doi.org/10.1016/j.sbi.2022.102460
41 Krempl, C., Lazzaretti, D. & Sprangers, R. A structural biology view on the enzymes involved in eukaryotic mRNA turnover. *Biological Chemistry* **404**, 1101-1121 (2023). https://doi.org/10.1515/hsz-2023-0182
42 Freund, E. C. *et al.* Efficient gene knockout in primary human and murine myeloid cells by non-viral delivery of CRISPR-Cas9. *Journal of Experimental Medicine* **217** (2020). https://doi.org/10.1084/jem.20191692
43 Evans, R. *et al.* Protein complex prediction with AlphaFold-Multimer. *bioRxiv* (2022). https://doi.org/10.1101/2021.10.04.463034
44 Mauxion, F. *et al.* The human CNOT1-CNOT10-CNOT11 complex forms a structural platform for protein-protein interactions. *Cell Reports* **42**, 111902 (2023). https://doi.org/10.1016/j.celrep.2022.111902
45 Gordon, D. E. *et al.* A Quantitative Genetic Interaction Map of HIV Infection. *Molecular Cell* **78**, 197-209.e197 (2020). https://doi.org/10.1016/j.molcel.2020.02.004
46 Fabian, M. R. *et al.* Structural basis for the recruitment of the human CCR4–NOT deadenylase complex by tristetraprolin. *Nature Structural & Molecular Biology* **20**, 735-739 (2013). https://doi.org/10.1038/nsmb.2572
47 Sedlyarov, V. *et al.* Tristetraprolin binding site atlas in the macrophage transcriptome reveals a switch for inflammation resolution. *Molecular Systems Biology* **12**, 868 (2016). https://doi.org/10.15252/msb.20156628
48 Mcguire, V. A. *et al.* Beta Interferon Production Is Regulated by p38 Mitogen-Activated Protein Kinase in Macrophages via both MSK1/2- and Tristetraprolin-Dependent Pathways. *Molecular and Cellular Biology* **37**, MCB.00454-00416 (2016). https://doi.org/10.1128/mcb.00454-16

49 Kovarik, P., Bestehorn, A. & Fesselet, J. Conceptual Advances in Control of Inflammation by the RNA-Binding Protein Tristetraprolin. *Frontiers in Immunology* **12** (2021). https://doi.org/10.3389/fimmu.2021.751313
50 Bulbrook, D. *et al.* Tryptophan-Mediated Interactions between Tristetraprolin and the CNOT9 Subunit Are Required for CCR4-NOT Deadenylase Complex Recruitment. *Journal of Molecular Biology* **430**, 722-736 (2018). https://doi.org/10.1016/j.jmb.2017.12.018
51 Sgromo, A. *et al.* A CAF40-binding motif facilitates recruitment of the CCR4-NOT complex to mRNAs targeted by Drosophila Roquin. *Nature Communications* **8**, 14307 (2017). https://doi.org/10.1038/ncomms14307
52 Collados Rodriguez, M. The Fate of Speckled Protein 100 (Sp100) During Herpesviruses Infection. *Front Cell Infect Microbiol* **10**, 607526 (2020). https://doi.org/10.3389/fcimb.2020.607526
53 Bloch, D. B. *et al.* Structural and Functional Heterogeneity of Nuclear Bodies. *Molecular and Cellular Biology* **19**, 4423-4430 (1999). https://doi.org/10.1128/mcb.19.6.4423
54 Bloch, D. B., De la Monte, S. M., Guigaouri, P., Filippov, A. & Bloch, K. D. Identification and characterization of a leukocyte-specific component of the nuclear body. *Journal of Biological Chemistry* **271**, 29198-29204 (1996). https://doi.org/10.1074/jbc.271.46.29198
55 Chelbi-Alix, M. K. & De Thé, H. Herpes virus induced proteasome-dependent degradation of the nuclear bodies-associated PML and Sp100 proteins. *Oncogene* **18**, 935-941 (1999). https://doi.org/10.1038/sj.onc.1202366
56 Madani, N. *et al.* Implication of the lymphocyte-specific nuclear body protein Sp140 in an innate response to human immunodeficiency virus type 1. *Journal of virology* **76**, 11133-11138 (2002). https://doi.org/10.1128/JVI.76.21.11133-11138.2002
57 Remick, B. C., Gaidt, M. M. & Vance, R. E. Effector-Triggered Immunity. *Annual Review of Immunology* **41**, 453-481 (2023). https://doi.org/10.1146/annurev-immunol-101721-031732
58 Jones, J. D. G., Staskawicz, B. J. & Dangl, J. L. The plant immune system: From discovery to deployment. *Cell* **187**, 2095-2116 (2024). https://doi.org/10.1016/j.cell.2024.03.045
59 Lopes Fischer, N. *et al.* Effector-triggered immunity and pathogen sensing in metazoans. *Nature Microbiology* **5** (2019). https://doi.org/10.1038/s41564-019-0623-2
60 Orzalli, M. H. & Parameswaran, P. Effector-triggered immunity in mammalian antiviral defense. *Trends in Immunology* **43**, 1006-1017 (2022). https://doi.org/10.1016/j.it.2022.10.004
61 Poetz, F. *et al.* RNF219 attenuates global mRNA decay through inhibition of CCR4-NOT complex-mediated deadenylation. *Nature Communications* **12** (2021). https://doi.org/10.1038/s41467-021-27471-6
62 Stumpo, D. J. *et al.* Chorioallantoic Fusion Defects and Embryonic Lethality Resulting from Disruption of *Zfp36L1*, a Gene Encoding a CCCH Tandem Zinc

Finger Protein of the Tristetraprolin Family. *Molecular and Cellular Biology* **24**, 6445-6455 (2004). https://doi.org/10.1128/mcb.24.14.6445-6455.2004

63 Stumpo, D. J. *et al.* Targeted disruption of Zfp36l2, encoding a CCCH tandem zinc finger RNA-binding protein, results in defective hematopoiesis. *Blood* **114**, 2401-2410 (2009). https://doi.org/10.1182/blood-2009-04-214619

64 Lai, W. S., Kennington, E. A. & Blackshear, P. J. Tristetraprolin and Its Family Members Can Promote the Cell-Free Deadenylation of AU-Rich Element-Containing mRNAs by Poly(A) Ribonuclease. *Molecular and Cellular Biology* **23**, 3798-3812 (2003). https://doi.org/10.1128/mcb.23.11.3798-3812.2003

65 Makita, S., Takatori, H. & Nakajima, H. Post-Transcriptional Regulation of Immune Responses and Inflammatory Diseases by RNA-Binding ZFP36 Family Proteins. *Frontiers in Immunology* **12** (2021). https://doi.org/10.3389/fimmu.2021.711633

66 Cook, M. E. *et al.* The ZFP36 family of RNA binding proteins regulates homeostatic and autoreactive T cell responses. *Science Immunology* **7** (2022). https://doi.org/10.1126/sciimmunol.abo0981

67 Popović, B. *et al.* Time-dependent regulation of cytokine production by RNA binding proteins defines T cell effector function. *Cell Reports* **42**, 112419 (2023). https://doi.org/10.1016/j.celrep.2023.112419

68 Petkau, G. *et al.* The timing of differentiation and potency of CD8 effector function is set by RNA binding proteins. *Nature Communications* **13** (2022). https://doi.org/10.1038/s41467-022-29979-x

69 Qiu, L.-Q., Stumpo, D. J. & Blackshear, P. J. Myeloid-Specific Tristetraprolin Deficiency in Mice Results in Extreme Lipopolysaccharide Sensitivity in an Otherwise Minimal Phenotype. *The Journal of Immunology* **188**, 5150-5159 (2012). https://doi.org/10.4049/jimmunol.1103700

70 Kratochvill, F. *et al.* Tristetraprolin-driven regulatory circuit controls quality and timing of mRNA decay in inflammation. *Molecular Systems Biology* **7** (2011). https://doi.org/10.1038/msb.2011.93

71 Snyder, B. L. *et al.* Synergistic roles of tristetraprolin family members in myeloid cells in the control of inflammation. *Life Science Alliance* **7**, e202302222 (2023). https://doi.org/10.26508/lsa.202302222

72 Lanz, T. V. *et al.* Clonally expanded B cells in multiple sclerosis bind EBV EBNA1 and GlialCAM. *Nature* **603**, 321-327 (2022). https://doi.org/10.1038/s41586-022-04432-7

73 Barton, E., Mandal, P. & Speck, S. H. Pathogenesis and Host Control of Gammaherpesviruses: Lessons from the Mouse. *Annual Review of Immunology* **29**, 351-397 (2011). https://doi.org/10.1146/annurev-immunol-072710-081639

74 Kjetil Bjornevik, M. C., Brian C. Healy, Jens Kuhle, Michael J. Mina, Yumei Leng, Stephen J. Elledge, David W. Niebuhr, Ann I. Scher, Kassandra L. Munger, Alberto Ascherio. Longitudinal analysis reveals high prevalence of Epstein-Barr virus associated with multiple sclerosis. *Science*, 296-301 (2022). https://doi.org/10.1126/science.abj8222

75 Wang, H. *et al.* One-Step Generation of Mice Carrying Mutations in Multiple Genes by CRISPR/Cas-Mediated Genome Engineering. *Cell* **153**, 910-918 (2013). https://doi.org/10.1016/j.cell.2013.04.025
76 Buenrostro, J. D., Wu, B., Chang, H. Y. & Greenleaf, W. J. ATAC-seq: A Method for Assaying Chromatin Accessibility Genome-Wide. *Current protocols in molecular biology* **109**, 21.29.21-29 (2015). https://doi.org/10.1002/0471142727.mb2129s109
77 Quinlan, A. R. & Hall, I. M. BEDTools: a flexible suite of utilities for comparing genomic features. *Bioinformatics* **26** (2010). https://doi.org/10.1093/bioinformatics/btq033
78 McLean, C. Y. *et al.* GREAT improves functional interpretation of cis-regulatory regions. *Nature Biotechnology* **28** (2010). https://doi.org/10.1038/nbt.1630
79 Elfmann, C. & Stülke, J. PAE viewer: a webserver for the interactive visualization of the predicted aligned error for multimer structure predictions and crosslinks. *Nucleic Acids Research* **51** (2023). https://doi.org/10.1093/nar/gkad350
80 Mei, S. *et al.* Cistrome Data Browser: a data portal for ChIP-Seq and chromatin accessibility data in human and mouse. *Nucleic Acids Research* **45**, D658-D662 (2017). https://doi.org/10.1093/nar/gkw983
81 Zheng, R. *et al.* Cistrome Data Browser: expanded datasets and new tools for gene regulatory analysis. *Nucleic Acids Research* **47**, D729-D735 (2019). https://doi.org/10.1093/nar/gky1094

Supplemental Figures

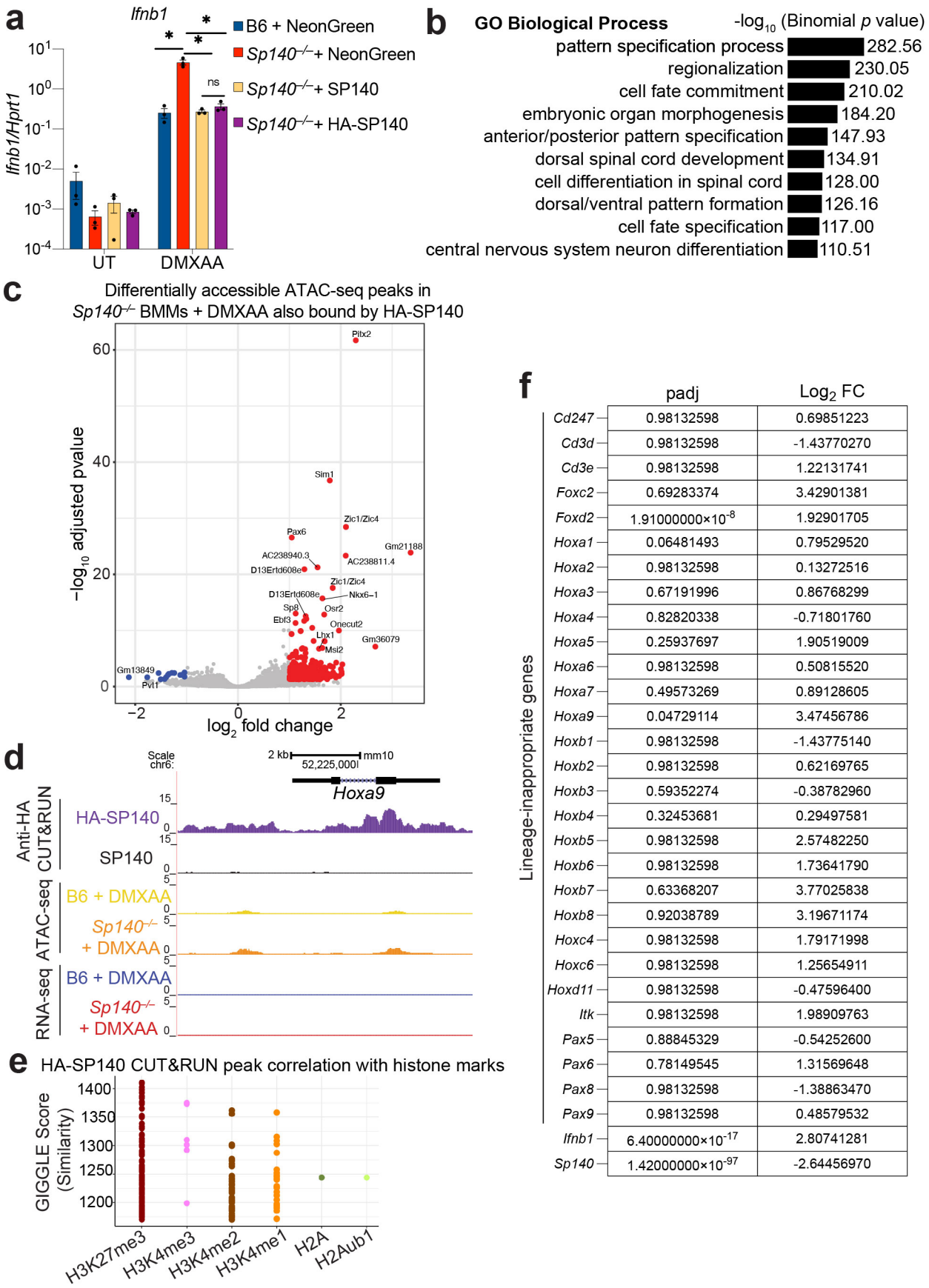

		padj	Log_2 FC
Lineage-inappropriate genes	*Cd247*	0.98132598	0.69851223
	Cd3d	0.98132598	-1.43770270
	Cd3e	0.98132598	1.22131741
	Foxc2	0.69283374	3.42901381
	Foxd2	1.91000000×10^{-8}	1.92901705
	Hoxa1	0.06481493	0.79529520
	Hoxa2	0.98132598	0.13272516
	Hoxa3	0.67191996	0.86768299
	Hoxa4	0.82820338	-0.71801760
	Hoxa5	0.25937697	1.90519009
	Hoxa6	0.98132598	0.50815520
	Hoxa7	0.49573269	0.89128605
	Hoxa9	0.04729114	3.47456786
	Hoxb1	0.98132598	-1.43775140
	Hoxb2	0.98132598	0.62169765
	Hoxb3	0.59352274	-0.38782960
	Hoxb4	0.32453681	0.29497581
	Hoxb5	0.98132598	2.57482250
	Hoxb6	0.98132598	1.73641790
	Hoxb7	0.63368207	3.77025838
	Hoxb8	0.92038789	3.19671174
	Hoxc4	0.98132598	1.79171998
	Hoxc6	0.98132598	1.25654911
	Hoxd11	0.98132598	-0.47596400
	Itk	0.98132598	1.98909763
	Pax5	0.88845329	-0.54252600
	Pax6	0.78149545	1.31569648
	Pax8	0.98132598	-1.38863470
	Pax9	0.98132598	0.48579532
	Ifnb1	6.40000000×10^{-17}	2.80741281
	Sp140	1.42000000×10^{-97}	-2.64456970

Supplemental Figure 1. SP140 predominantly represses chromatin accessibility

and binds genes involved in development, although these genes are not differentially expressed in the absence of SP140.

a. RT-qPCR for *Sp140*$^{-/-}$ BMMs retrovirally transduced with indicated constructs, treated with 100 μg/mL DMXAA for 8 hours.
b. Top 10 GO terms for genes bound by HA-SP140 in anti-HA CUT&RUN.
c. Volcano plot of differentially accessible ATAC-seq peaks in DMXAA-treated *Sp140*$^{-/-}$ vs. B6 BMMs, filtered by genes that are also bound by HA-SP140 in anti-HA CUT&RUN. Blue dots indicate genes with $\log_2$ fold change < -1 and adjusted *p* (padj) < 0.05, and red dots indicate genes with $\log_2$ fold change > 1 and padj < 0.05. for differential ATAC-seq peak accessibility in *Sp140*$^{-/-}$ BMMs treated with DMXAA.
d. Alignment of reads from HA-SP140 or untagged SP140 anti-HA CUT&RUN, and RNA-seq/ATAC-seq of *Sp140*$^{-/-}$ and B6 BMMs treated with DMXAA at *Hoxa9.*
e. GIGGLE similarity score for overlap of HA-SP140 CUT&RUN peaks with publicly available ChIP-seq datasets for indicated histone marks[80,81].
f. Table of adjusted *p* (padj) and $\log_2$ fold change for "lineage-inappropriate SP140-regulated" genes[17] from RNA-seq of DMXAA-treated *Sp140*$^{-/-}$ and B6 BMMs.

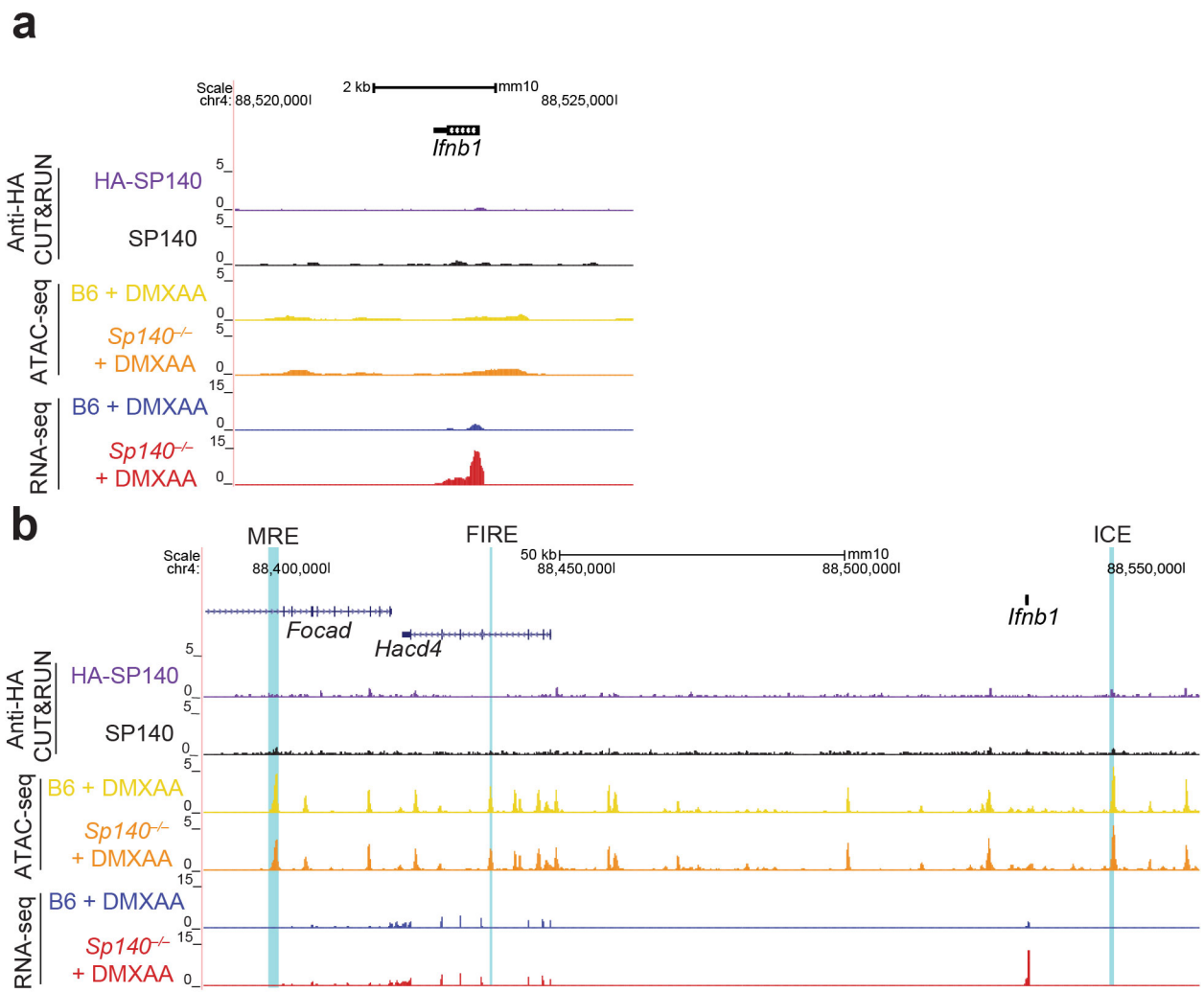

Supplemental Figure 2. SP140 does not bind the *Ifnb1* locus or known regulatory elements.

a. Alignment of reads at *Ifnb1* from HA-SP140 or untagged SP140 anti-HA CUT&RUN, ATAC-seq of DMXAA-treated *Sp140*$^{-/-}$ and B6 BMMs, and RNA-seq of DMXAA-treated *Sp140*$^{-/-}$ and B6 BMMs.
b. Alignment of reads from HA-SP140 or untagged SP140 anti-HA CUT&RUN, and ATAC-seq/RNA-seq of *Sp140*$^{-/-}$ and B6 BMMs treated with DMXAA, at the *Ifnb1* regulatory elements ICE[34,35], FIRE[33], and the MRE[32].

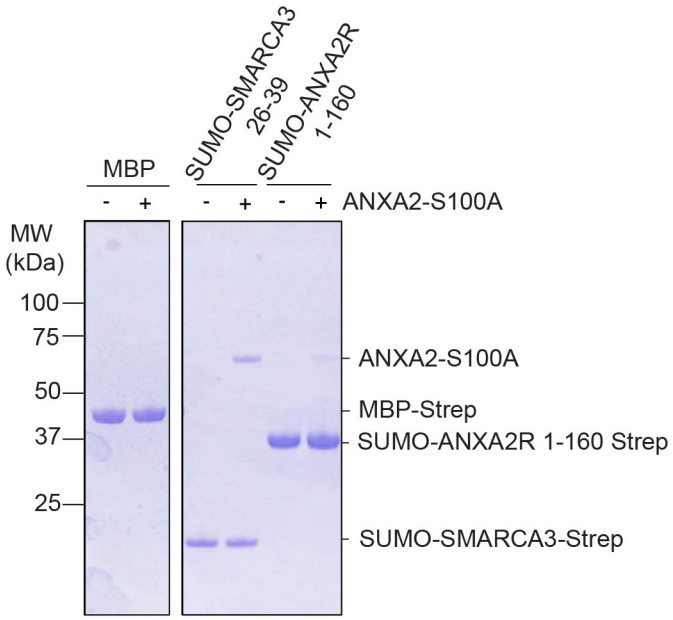

Supplemental Figure 3. RESIST1-160 does not bind ANXA2-S100A.
Pull-down assay with recombinant His6-SUMO-ANXA2R (residues 1-160) and SUMO-SMARCA3 (residues 26-39) tagged with a StrepII (Strep) affinity tag upon incubation with ANXA2-S100A.

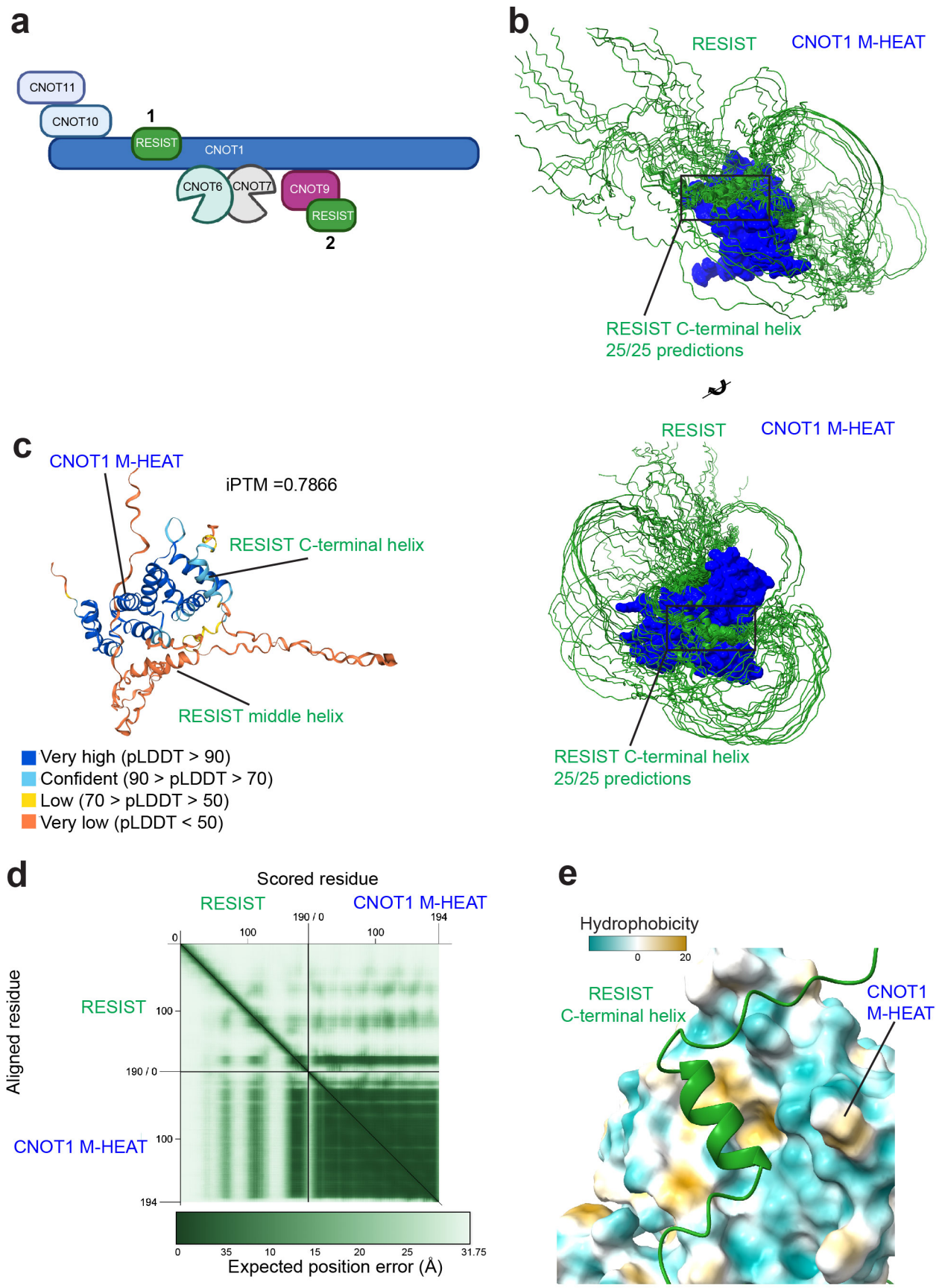

Supplemental Figure 4. AlphaFold predictions suggest RESIST likely binds the

CNOT1 M-HEAT domain.

a. Schematic of CCR4-NOT subunit and RESIST complexes produced by Alphafold Multimer.
b. Aligned AlphaFold models of RESIST with the CNOT1 M-HEAT domain.
c. The top-scoring structural prediction of the RESIST and CNOT1 M-HEAT complex, colored by pLDDT.
d. AlphaFold PAE plot of predicted RESIST and CNOT1 M-HEAT complex. Plot generated with PAEViewer[79].
e. Depiction of RESIST binding to a hydrophobic patch on the CNOT-1 M-HEAT domain (CNOT1 colored by hydrophobicity).

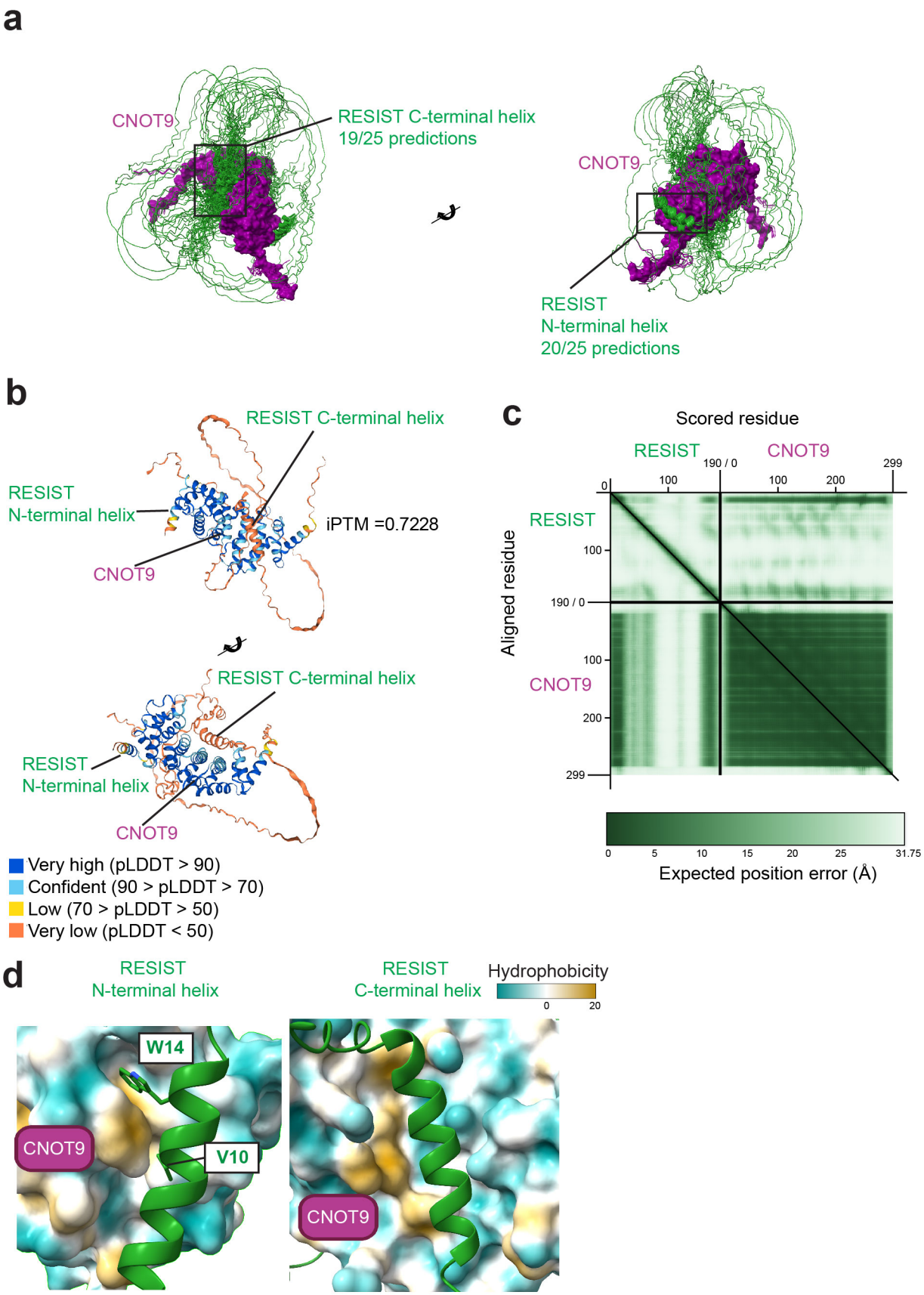

Supplemental Figure 5. AlphaFold predictions suggest RESIST likely binds the

CNOT9 subunit.

a. Aligned structural predictions of RESIST interactions with CNOT9.
b. Second-ranked Alphafold structural prediction of RESIST and CNOT9 complex colored by pLDDT.
c. AlphaFold PAE plot of predicted RESIST and CNOT9 complex. Plot generated with PAEViewer[79].
d. Depiction of RESIST binding to multiple hydrophobic patches on CNOT9 (CNOT9 colored by hydrophobicity).

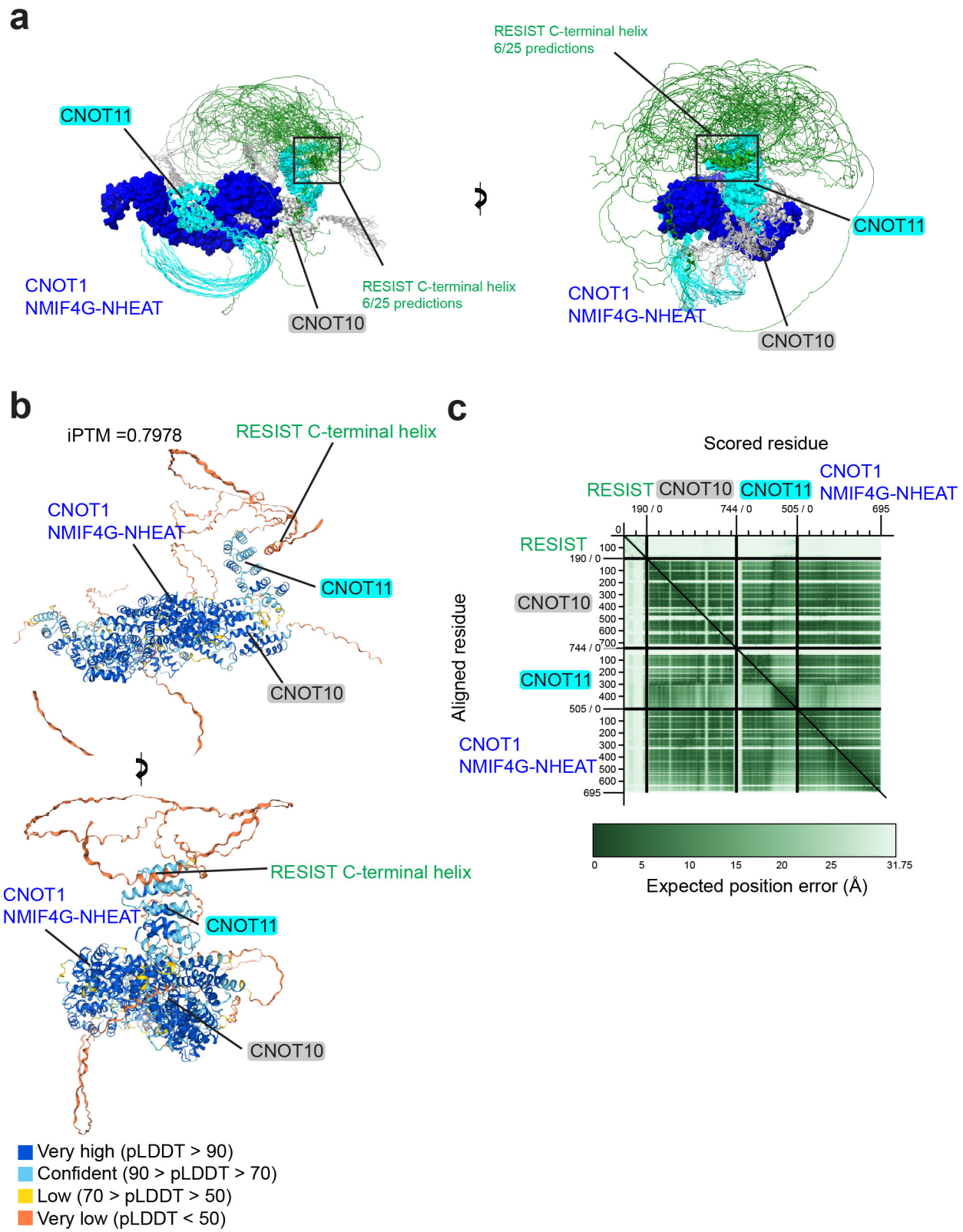

Supplemental Figure 6. AlphaFold predictions suggest RESIST likely does not bind CNOT11.

a. Aligned AlphaFold structure predictions of RESIST with the CNOT1 NMIF4G-NHEAT domains, CNOT10, and CNOT11.
b. Highest-scoring AlphaFold structure prediction of RESIST and CNOT1/CNOT10/CNOT11 complex colored by pLDDT.
c. AlphaFold PAE plot of predicted RESIST and CNOT1/CNOT10/CNOT11 complex. Plot generated with PAEViewer[79].

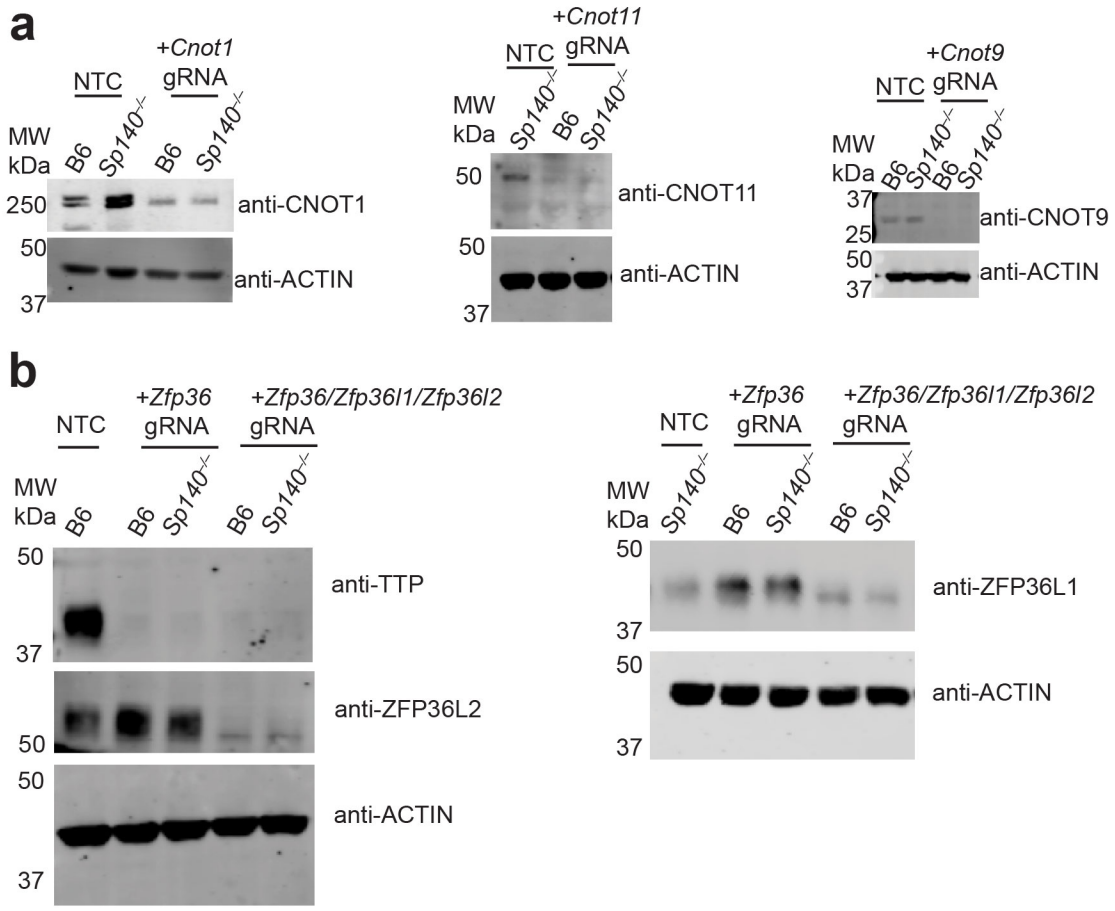

Supplemental Figure 7. Assessment of CCR4-NOT subunit and TTP family knockout efficiency.

a. Immunoblot of B6 or *Sp140*$^{-/-}$ BMMs electroporated with indicated gRNAs for indicated CCR4-NOT subunits for experiments shown in Fig. 4b.
b. Immunoblot of B6 or *Sp140*$^{-/-}$ BMMs electroporated with indicated gRNAs for indicated TTP family members for experiments shown in Fig. 4e after 8 hours of 100 μg/mL DMXAA.

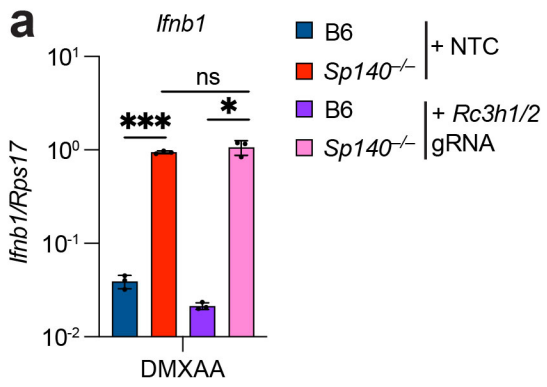

b

ICE Analysis KO score
(% of indels producing producing frameshift)

Gene	B6	*Sp140*$^{-/-}$
Rc3h1	85	82
Rc3h2	88	84

Supplemental Figure 8. Roquin does not regulate *Ifnb1* in BMMs.

a. RT-qPCR for *Ifnb1* in BMMs electroporated with indicated gRNAs after 8 hours of 100 μg/mL DMXAA treatment.
b. Knockout efficiency for *Rc3h1*/*Rc3h2* in BMMs electroporated with gRNAs targeting *Rc3h1* and *Rc3h2* for results shown in a.

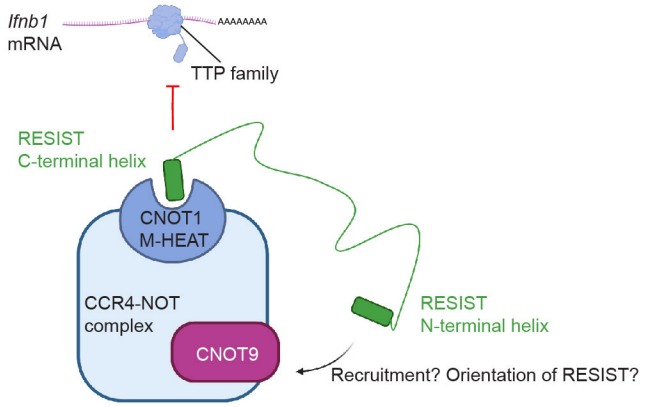

Supplemental Figure 9. A proposed model for the mechanism of RESIST-mediated *Ifnb1* stabilization. Schematic for how RESIST may interact with CCR4-NOT subunits CNOT1 and CNOT9 to mediate stabilization of *Ifnb1* mRNAs.

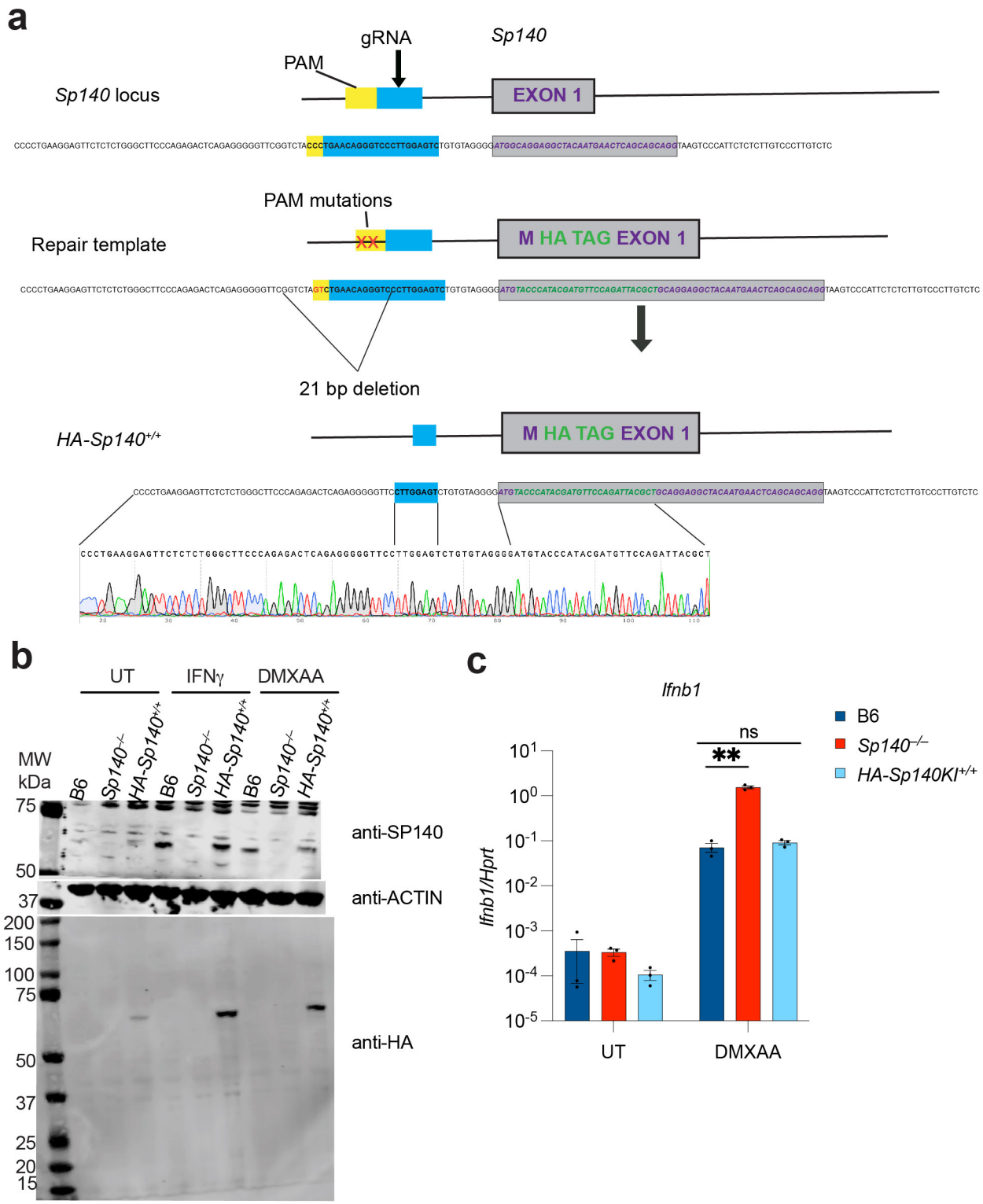

Supplemental Figure 10. Generation and validation of *HA-Sp140* knock-in mice.

a. Schematic of gene-targeting strategy to generate *HA-Sp140* knock-in mice and depiction of resulting *HA-Sp140*$^{+/+}$ founder line.

b. Immunoblot of BMMs of indicated genotypes treated with 100 μg/mL DMXAA for 8 hours or 10 ng/mL IFNγ for 24 hours.
c. RT-qPCR for *Ifnb1* from BMMs of indicated genotypes after 8 hours of 100 μg/mL DMXAA treatment.

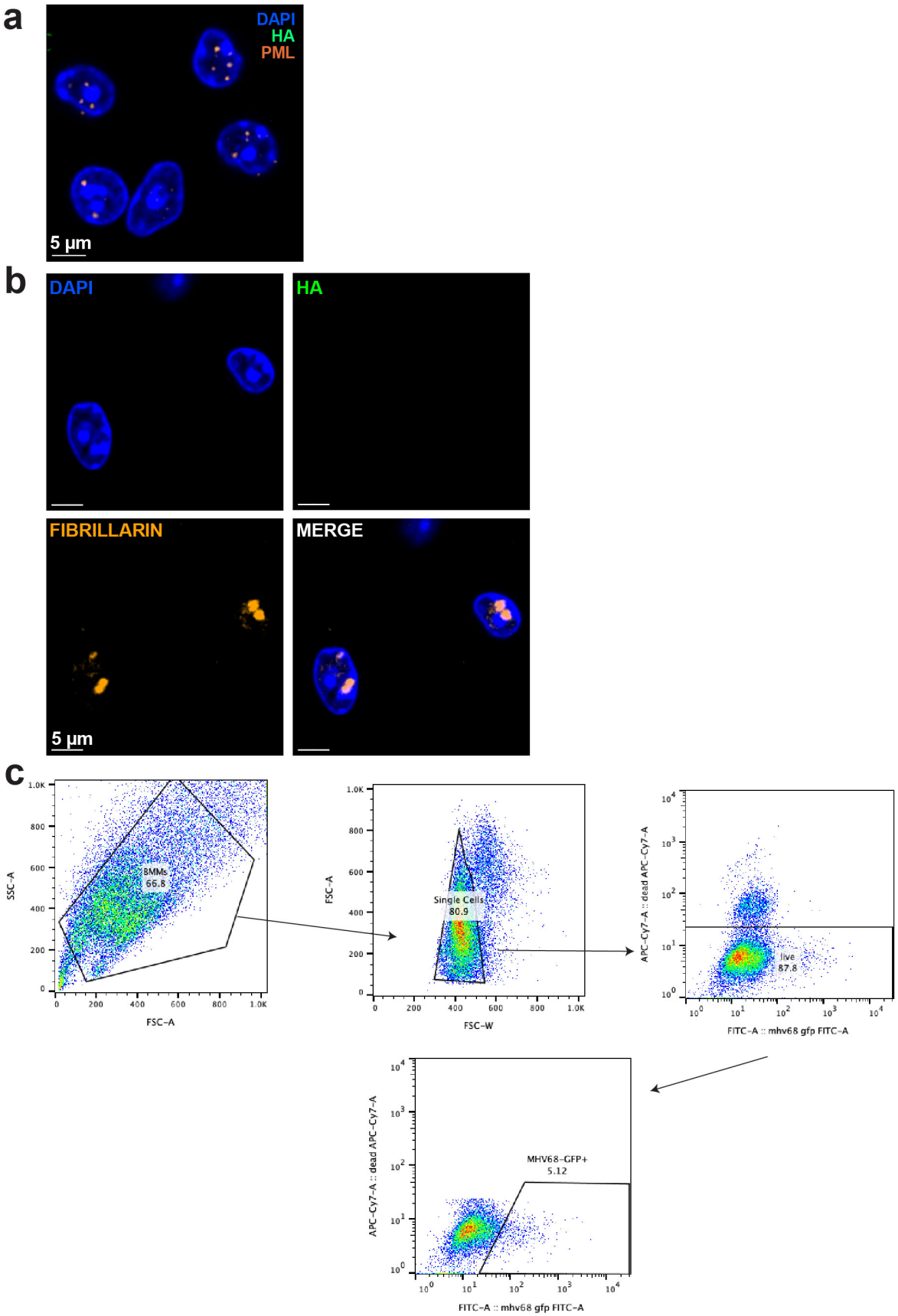

Supplemental Figure 11. B6 BMM IF staining controls and gating strategy for

MHV68-GFP BMMs.

a. Immunofluorescence of B6 BMMs treated with 8 hours of 100 μg/mL DMXAA stained with anti-HA, anti-PML, and DAPI.
b. Immunofluorescence of B6 BMMs treated with 8 hours of 100 μg/mL DMXAA stained with anti-HA, anti-fibrillarin, and DAPI.
c. Representative flow plots and gating strategy for B6 BMMs infected with MHV68-GFP, MOI 3, for 24 hours.